UNIVERSITY OF HELSINKI REPORT SERIES IN PHYSICS

HU-P-D116

CARDIAC MAGNETIC RESONANCE IMAGING TECHNIQUES IN THE ASSESSMENT OF FLOW AND VOLUMETRY

Veli-Pekka Poutanen

Department of Physical Sciences
Faculty of Science
University of Helsinki
Helsinki, Finland

ACADEMIC DISSERTATION

To be presented, with the permission of the Faculty of Science of the University of Helsinki, for public criticism in Auditorium D101 of the Department of Physical Sciences (Physicum), Gustaf Hällströmin katu 2, On August 20th, 2004, at 12 o'clock noon.

Helsinki 2004

ISSN 0356-0961
ISBN 952-10-1661-2
ISBN 952-10-1662-0 (pdf-version)
http://ethesis.helsinki.fi/
Helsinki 2004
Yliopistopaino

‘Everything flows and nothing stays”

Heraclitus

V-P. Poutanen: Cardiac Magnetic Resonance Imaging in the assessment of flow and volumetry, University of Helsinki, 2004, 67 p. + appendices, University of Helsinki, Report Series in Physics, HU-P-D116, ISSN 0356-0961, ISBN 952-10-1661-2, ISBN 952-10-1662-0 (pdf-version).

Classification (INSPEC): A3325, A4110F, A7500, A75406, B5100, B5310
Keywords: medical physics, magnetic resonance imaging, cardiac MRI, phantom, MR velocity mapping, pulsatile blood flow, heart function, heart volume.

ABSTRACT

With ever-shortening acquisition times and electrocardiographic (ECG) gating, magnetic resonance imaging (MRI) applications have been extended to the examination of organ function. In cine cardiac MRI, heart motion can be frozen at certain phases in the cardiac cycle to obtain information on the morphology as well as functioning of the heart. Consecutive images can then be viewed dynamically to depict motion. MRI allows direct measurement of flow with an appropriate MR velocity-sensitive pulse sequence. The segmented spoiled gradient echo sequences, which acquire several k-space lines in each cardiac phase, provide high-resolution dynamic images in a single breath-hold, thus avoiding respiratory artifacts. The purpose of the present study is to investigate the accuracy of conventional and breath-hold cine phase-contrast-interleaved imaging sequences with phantom measurements and apply the technique to study 3-D flow profiles at the left ventricular outflow tract during systole and at the mitral annulus during diastole. Conventional velocity-mapping sequences were also applied to assess the flow-wave velocity (FWV) in the aorta. FWV was chosen as an index of aortic stiffness. The aim was to assess the reduction in aortic stiffness with antihypertensive treatment. Nonvelocity-sensitive cine MRI was applied to develop and validate a method for studies of human atrial and right ventricular volumes and function.

Nonvelocity-sensitive MRI was used to evaluate right atrial volumes (casts) using a spin-echo (SE) sequence and right ventricle (cast) using a gradient echo (GRE) sequence (FLASH). The aim of the right ventricular study was to identify the optimal imaging plane for the right ventricle. The right and left atrial volume cycles in healthy subjects was determined, using a GRE cine sequence (FISP).

The phantom study with three steady flows (10, 20, and 25 ml/s) shows good correlation between the theoretical mean velocities (31, 62, 78 cm/s) and the measured velocities. In pulsatile flow, the velocity curves shifted in time ((linear fit; time = -10.1 x lines per segment (LPS) + 268 (R^2 = 0.99)) and flow curves smoothed when LPS was increased. The spatial inhomogeneity of the peak systolic velocity across the subaortic annular flow area, calculated as the percentage ratio of the range of the regional measurements about their mean, averaged 18.2 $\pm$ 5.0%, and the inhomogeneity of the mean flow rate was 19.2 $\pm$ 3.5%. In the mitral flow profile the spatial velocity of the individual spatial inhomogeneity averaged 33.5 $\pm$ 13.8% for the early velocity peak (range 14.3-56.2%), 41.1 $\pm$ 16.1% for the late diastolic velocity peak (range 10.5-60.0%) and 70.0 $\pm$ 33.9% for the mean diastolic flow rate (range

11.0-147.1%). The FWV in the thoracic aorta of patients with essential hypertension was reduced, but the changes were not statistically significant.

In the ascending aorta the luminal size and Peterson's aortic elastic modulus (E_p) decreased and the strain increased during the 6-month period of antihypertensive treatment. A series of 14 cadaveric human right atrial casts were examined. The volumes of the right atrial casts (64-187 ml) correlated closely ($R = 0.99$, $P < 0.001$) with the true volumes (70-206 ml) and atrial casts ranging from 19 to 119 ml correlated well with those true volumes varying from 19 to 113 ml. The right atrial volumes and volumetric function in healthy subjects showed that the maximum right atrial volume averaged 148 $\pm$ 26 ml and minimum 72 $\pm$ 18 ml. The minimum, maximum, reservoir, and stroke volumes were larger and ejection fraction smaller in the right atrium than in the left atrium. There were no statistically significant differences between the measured and true right ventricular volumes.

In vitro flow measurements suggested that conventional and segmented k-space cine MRI phase-contrast velocity mapping can be used for accurate flow quantification under conditions of steady and pulsatile flow. Conventional phase-contrast velocity mapping can be applied to measure flow profiles inside the heart and FWVs in the aorta. Both the transmitral flow profile in diastole and flow profile in the left ventricular outflow tract in systole were consistently skewed in healthy subjects. The FWV in the thoracic aorta decreased with both treatments, although the changes did not attain statistical significance. Aortic stiffness determined with cine MRI indicates that both drugs used improved the elastic function of the ascending thoracic aorta on essential hypertension. A cine GRE sequence can be successfully applied in cardiac right atrial studies in vivo. The normal right atrium was larger and its volumetric changes larger than those of the left atrium. The volumes of the 14 human cadaveric left and right atrial casts measured with SE sequence correlated closely with the true atrial volumes. Studies with human casts suggest that GRE sequence is well applicable to right ventricular volume measurements.

TABLE OF CONTENTS

LIST OF ORIGINAL PUBLICATIONS

This thesis is based on the following publications, which are referred to in the text by their Roman numerals I-VI

I Poutanen V.-P., Kivisaari R., Häkkinen A.-M., Savolainen S., Hekali P., Standertskjöld-Nordenstam C.-G. Multiphase segmented k-space velocity mapping in pulsatile flow waveforms, Magnetic Resonance Imaging, 16(3):261-270, 1998.

II Kupari M., Hekali P., Poutanen V.-P. Cross sectional profiles of systolic flow velocities in left ventricular outflow tract of normal subjects, British Heart Journal, 74(1):34-39, 1995.

III Kupari M., Järvinen V., Poutanen V.-P., Hekali P. Skewness of instantaneous mitral transannular flow-velocity profiles in normal humans, American Journal of Physiology, 268(3):1232-1238, 1995.

IV Savolainen A., Keto P., Poutanen V.-P., Hekali P., Standertskjöld-Nordenstam C.-G., Remes A., Kupari M. Effects of angiotensin-converting enzyme inhibition versus [beta]-adrenenergic blockade on aortic stiffness in essential hypertension, Journal of Cardiovascular Pharmacology, 27(1): 99-104, 1996.

V Järvinen V., Kupari M., Hekali P., Poutanen V.-P. Right atrial MR imaging studies of cadaveric casts and comparison with right and left atrial volumes and function in healthy subjects, Radiology, 191(1):137-142, 1994.

VI Jauhiainen T., Järvinen V., Hekali P., Poutanen V.-P., Penttilä A., Kupari M. MR gradient echo analysis of human cardiac casts: focus on the right ventricle, Journal of Computer Assisted Tomography, 22(6): 899-903, 1998.

Statement of involvement

All publications included in this thesis are the result of combined effort. The accuracy of conventional and segmented cine MR velocity mapping was planned and accomplished mainly by the author (V.-P. Poutanen), who programmed sequences for MR velocity mapping and tested and analyzed the MR-data (I). In other studies (II – VI) the author was the only physicist in the research team. The author analyzed the factors governing the accuracy and precision of MR flow measurements (II, III). The author combined this knowledge with prior information on the diameter of the target vessel and prevailing flow condition to define a protocol for measuring flow with negligible error. All the flow sequences in this work were designed by the author. The author planned and suggested the postprocessing methods. The author performed the validation measurements with phantom experiments (III) and was involved in protocol development in both flow-independent and flow-dependent acquisitions (IV-VI). The author made the transferring program from the MRI console to the off-line workstation and planned the analysis methods (IV, V).

SYMBOLS AND ABBREVIATIONS

ΔA	cross-sectional area variation
A	area
α	excitation pulse
ACE	angiotensin-converting enzyme
AIT	available imaging time
A_g	area of each lobe of the bipolar gradient
$\mathbf{a}_0$	acceleration of fluid at beginning of gradient waveform
B_o	magnetic flux density of the scanner's main magnetic field
β	stiffness index
BFFE	balanced fast field echo
CBASS	completely balanced steady state
CD	complex difference
CNR	contrast-to-noise ratio
CSE	conventional spin echo
CSF	cerebro-spinal fluid
D	distensibility
ECG	electrocardiography
EPI	echo planar imaging
ETL	echo train length
E_ρ	elastic modulus
FA	flip angle
FFE	fast field echo
FFT	Fourier flow technique
FIESTA	fast imaging employing steady-state acquisition
FISP	fast imaging with steady precession
FLASH	fast low angle shot
FOV	field of view
FSE	fast spin echo
FWV	flow-wave velocity
G_{read}	frequency-encoding gradient
$\Delta\phi$	phase shift, phase offset
ϕ	phase of received signal
G(t)	magnetic field gradient
GRASS	gradient-recalled acquisition into steady state
GRE	gradient echo
γ	magnetogyric ratio (γ = 2,67519 x 10^8 rad s^{-1} T^{-1} for protons)
LPS	lines per segment
MnCl	manganese chloride
MR	magnetic resonance
MRI	magnetic resonance imaging
M_1	first moment of the gradient waveform
ΔM_1	net gradient first moment
N	number of k-space lines
N_{acq}	number of acquisition
N_p	number of phases
O_2	oxygen
Pa	Pascal (N/m^2)

PAT	parallel acquisition technique
PC	phase contrast
PD	phase difference
PCVM	phase contrast velocity mapping
PSF	point spread function
PWV	pulse-wave velocity
ΔQ	flow variation
Q	flow
RF	radiofrequency
ROI	region of interest
$\mathbf{r}_0$	position of fluid at the beginning of gradient waveform
r(t)	position at time t
ρ	blood density
SE	spin echo
SENSE	sensitivity encoding
SNR	signal-to-noise ratio
SMASH	simultaneous acquisition of spatial harmonics
SPECT	single photon emission computed tomography
SPGR	spoiled gradient refocuses acquisition into steady state
SSFP	steady state free precession
Δt	transit time
T	Tesla (unit of magnetic flux density)
TE	echo time
T1	longitudinal relaxation time
T2	transverse relaxation time
TD	trigger delay
TOF	time of flight
TR	repetition time
TTL	transistor-transistor logic
TW	trigger window
T_s	total imaging time
T	time between the centers of two lobes of gradient
UHDC	University Hospital Development Corporation
θ_E	Ernst angle
VCG	vector cardiogram
Venc	velocity-encoding parameter
VNR	velocity-to-noise ratio
v_{mean}	mean velocity
$\mathbf{v}_0$	velocity of fluid at beginning of gradient waveform
Δx	distance between measurement locations

1 PURPOSE OF THE STUDY

The aim of the study was to explore and develop MR sequences for measuring flow inside the heart, in the aorta and in the coronary arteries. A procedure for assessing the volumes and the function of cardiac cavities was also developed. The specific aims were:

1) to investigate the accuracy of conventional and segmented cine MR velocity-mapping sequences in measuring steady and pulsatile flow in phantom (I),

2) to apply cine MR velocity mapping to measure flow profiles at the left ventricular outflow tract and at the mitral annulus (II and III),

3) to assess the degree of aortic distensibility using cine MRI (IV),

4) to use cine MRI for developing and validating a method for studies of human atrial and right ventricular volumes and function (V and VI).

2 INTRODUCTION

The chest roentgenogram remains the primary method for evaluation of cardiac diseases in most cases. However, this technique is relatively inaccurate and renders little information of function. Cardiac catheterization and angiography precisely depict the internal anatomy of the heart, define location and presence of disease, and allow pressure measurements. This invasive method results in serious complications in 1-3% of cases [1]. With new multidetector computer tomography (CT) it is possible to acquire high resolution three dimensional images of the heart and vessels. All the methods above use ionizing radiation and has several other drawbacks, including potential contrast reaction and lack of soft tissue contrast.

Functional information on the heart is critical for a complete understanding of the physiological impact of various lesions. Echocardiography and Doppler examinations are noninvasive techniques to study patients with known or suspected cardiac diseases and they are important tools for evaluating the anatomy and function of the heart. In real time, echocardiography provides considerable information on the motion of cardiac structures. It remains the method of choice in clinical practice due to wide machine availability, relatively low cost, and short examination times.

Gated single photon emission computed tomography (SPECT) can be used to measure cardiac function. However, gated SPECT is affected by changes in background activity and injected dose, which lead to overestimation of ventricular volumes [2]. Positron emission tomography (PET) measures metabolism and has important role when cardiac viability is assessed. Functional PET images can be fused to structural MR and CT images.

Magnetic resonance imaging (MRI) scanners have primarily been designed for use with the central nervous system, which is relatively free of motion. Thus, imaging times of several minutes duration have been acceptable. The fast technical development of MRI, however, has contributed MRI to become the imaging procedure of choice for assessment of cardiac structure and function. The two techniques that have given most information are: 1) cine MRI, where moving images of heart are obtained throughout the entire cardiac cycle in any desired orientation and 2) MR phase-contrast velocity mapping (PCVM) which permits quantitative calculation of blood flow in any spatial direction.

Flow effects in magnetic resonance imaging

The first non-imaging work indicating that flow measurement with MR would be possible was presented in 1959 [3]. Observations of the effect of flow on the magnetic resonance signal has also been reviewed by Jones and Child [4] and by Zhernovoi and Latyshev [5], but they did not suggest a method of flow measurement.

The same effect influence**s** the signal in the images as in the non-imaging experiments. Several methods have been proposed for imaging the flow phenomena. The methods can be divided into wash-in/wash-outflow methods [6, 7], time of flight (TOF) methods [8] and phase shift methods [9].

Wash-in/wash-outflow and TOF methods provide some information about the presence of flow. However, this information is only qualitative because the signal intensity of flowing fluid has a complicated dependence on sequence parameters, flow directions and relaxation times.

The most successful technique for flow measurement in clinical application has proven to be velocity phase encoding method [10]. Van Dijk [11] and Bryant and colleagues [12] first demonstrated the clinical use of velocity phase encoding. PCVM measures blood flow in one direction by obtaining two complete set of raw MR data using different gradient first moment in the direction of flow [13]. PCVM method creates an image in which pixel intensity depends on the mean velocity of the spins inside the pixel.

Cine MRI using short repetition time (TR) gradient echo sequences and cardiac gating can be used for imaging dynamic processes. By combining PCVM and cine MR a technique that can depict motion and flow throughout the cardiac cycle can be produced [14].

In the present study cine MRI was used to quantify the diastolic and systolic cross-sectional areas and aortic distensibility (IV). The volumes of the right and left atrium and right ventricle were assessed, using cine MRI and the method of disks.

Here, we examined the accuracy of conventional and segmented cine MR PCVM sequences. According to the best knowledge of authors, prior to this study no comprehensive data has been available of the accuracy of segmented PCVM applied to pulsatile flow patterns. In addition the applicability of velocity-sensitive cine MRI in velocity profiles and an aortic flow wave velocity (FWV) and the general nonvelocity sensitive cine in aortic compliance and cardiac volumetry were evaluated. Complete cross-sectional velocity profiles at the left ventricular outflow tract and mitral annulus (II, III) have not been previously reported. PCVM was used to measure the aortic FWV in patients with essential hypertension (IV).

3 CARDIAC APPLICATIONS OF CINE MRI

For cardiac imaging time resolution of the order 25 - 50 ms is needed. Using the cardiac-gated acquisition, MR images of the heart are restricted to a constant phase of the cardiac cycle. This method reduces the artifacts caused by flow and the complex motion of the heart. MRI can provide high contrast between moving blood and the myocardium, has high spatial resolution, and does not make any use of ionizing radiation.

Cine PCVM provides a 2-D series of velocity images and is applicable to most vessels. Cine PCVM provides analyses of pulsatile arterial flow over cardiac cycle. In the pulmonary, coronary, and renal vasculature, respiratory motion artifacts tend to degrade image quality and accuracy of flow measurements.

3.1 Valvular heart disease

Doppler echocardiography is used in conjunction with a simplified Bernoulli equation to measure transvalvular pressure gradients in diagnosing valve stenosis severity [15]. Studies have shown that Doppler-based measurements tend to have low precision [16-18]. MRI has become a complimentary modality to echocardiography for the evaluation of valvular disease.

MRI is rapidly gaining acceptance as an accurate, reproducible, noninvasive method for assessment of structural and functional parameters in patients with valvular heart disease. The severity of valvular regurgitation can be evaluated with cine GRE imaging, which allows measurement of the area of signal void due to a intravoxel dephasing of spins with subsequent cancellation of the net signal [19]. This phenomenon can be used to visualize regurgitant and stenotic flow jets [20]. MRI can also be used for assessment of stenosis severity via peak velocity determination [21].

PCVM can be used to assess aortic and mitral regurgitation. However, results of the PCVM measurement in aortic regurgitation are dependent on the slice position [22]. Multiple slices are needed to measure mitral regurgitation due to the interaction between the regurgitant flow field and the aortic outflow field in the left ventricular cavity [22]. Measuring aortic regurgitation with a single imaging slice by positioning the slice between the aortic valve annulus and the coronary ostia was proven to minimize the influence of coronary flow and aortic compliance on the accuracy of measured diastolic flow [22]. However, problems in accurate measurement are caused by movement; the basal left ventricular points move as much as 12 mm in the long axis direction during diastole [23]. It was also suggested that PCVM for aortic regurgitation is most reliably performed near the aortic valve [24]. The large acceleration immediately proximal to the orifice and turbulent jet flow distal to the orifice, both of which can lead to severe signal loss, may cause additional problems in quantitative assessment of flow rate.

3.2 Assessment of flow profiles

MRI can be easily applied to obtain flow profiles through arbitrary planes in the peripheral and central vessels. The results of the PCVM measurement can be represented with 3-D wire-frame representations at different times in the cardiac cycle. These can be used to evaluate fine flow detail that could otherwise escape notice. The wire-frames can be viewed in a cineloop, or static set.

Spatially complete cross-sectional velocity maps could not be produced by Doppler method. Velocity-encoded cine MRI enables noninvasive determination of flow profiles across any section of the heart or great vessels [25]. The velocity encoded phase images show the velocity of the spins in each individual voxel of the image.

3.3 Aortic compliance estimation

Compliance is one of the important parameters of the arterial wall used to estimate risk for vascular diseases [26]. The elastic properties of the great arteries determine the pulsatile component of the afterload and influence the performance of the left ventricle, especially when ventricular dysfunction is present, and may also modify the aorta-coronary blood flow [27-29]. Previous studies determined the aortic pressure with invasive local intravascular measurements [30]. MRI provides a noninvasive method for evaluating compliance and related PWVs of the ascending aorta.

MRI's usefulness in the study of aortic distensibility (D) is well documented [27, 31]. The thoracic aorta may also stiffen in other acquired or congenital diseases [32] and in certain inherited disorders of connective tissue, such as the Marfan syndrome [33, 34]. Atherosclerosis, hypertension, aneurysm formation, and normal ageing play a significant role in the biophysical properties of the aortic wall.

Frame by frame images of the smallest and largest circumferences of the ascending and descending thoracic aorta can be selected while scrutinizing cine loops acquired by cardiac triggered cine-examination. These measurements can be used to calculate the number of indices describing regional aortic function: i.e. compliance: change in the slice volume/pulse pressure, D: cross-sectional area strain/pulse pressure, elastic modulus (E_ρ): pulse pressure/area strain, stiffness index (β): (systolic blood pressure/diastolic blood pressure)/area strain [26, 35, 36].

The elastic properties of arterial vessels are very important in cardiovascular hemodynamics. PVW is directly related to the elastic properties of the vessel wall. Distensibility D can be computed for a given PWV:

$$D = 1/\rho c^2, \qquad (1)$$

where ρ is the blood density and c the PWV.

Several methods have been proposed for PVW measurement, most of them based on PC techniques [37, 38]. PWV, i.e. the rate of propagation of flow or pressure in the arteries, is directly related to the stiffness of the aorta. The less distensible the aorta, the higher the PWV and therefore it can be used together with aortic

compliance as indices for the risk of pathologic changes such as atherosclerosis. Cine MR PWV measurement has been proposed as a method for non-invasively determining compliance, using the direct relationship between PWV and compliance. PVW and aortic compliance are important determinants of heart load. PWV can be calculated from equation

$$PWV = \Delta Q/\Delta A, \qquad (2)$$

where ΔQ is flow variation and ΔA the variation of cross-sectional area. In another method PWV is calculated using the transit time (Δt) of the foot of the flow wave across the aortic arch and the distance (Δx) between the locations of both measurements [39]:

$$PWV = \Delta x/\Delta t, \qquad (3)$$

Thus, PWV can be estimated by performing time-resolved MR PC flow measurements at different positions along the length of the vessel.

Traditionally MR measurements of PWV require data to be collected over multiple heartbeats [40]. The MR-tagging approach can provide an independent measurement of the PWV for each heartbeat, making it insensitive to potential triggering errors [41].

3.4 Assessment of global and local cardiac function

MRI can be used as truly three-dimensional method to assess cardiac cavities without the need of contrast media. The increase in spatiotemporal resolution of MRI has made it possible to acquire high-resolution volumetric cardiac image data as a function of time. Cardiac chamber volumes have been validated in vitro models by measuring latex casts of excised human left ventricles [42]. Cardiac MRI volumetric studies have been first validated using gated SE sequence of cast volumes, cadaveric hearts and free-breathing animals [43-47]. Cine GRE imaging has been found to be an accurate and reproducible method for assessment of left ventricular volumes, mass, and function in vitro and in vivo studies [46, 48-51]. Complete atrial and right ventricular volume curves and studies on optimal imaging view for the right ventricular volumetric studies with MRI are few [52,57].

The two principle obstacles to be overcome in the MR methods for assessment of cardiac chamber volume have been reliable cardiac gating and long acquisition times. We have used a simplified area-based method to assess cardiac function [53]. Several other methods for estimating ventricular volumes using limited geometric data have been suggested [54, 55]. Of these the biplane Simpson's rule approach, which treats the ventricle as a solid of revolution, is most reliable, and the single-plane area length method least reliable [56].

One way to reconstruct the three-dimensional volume is to image adjoining image-planes that have certain thickness and to sum up the volume of the object in each section (the method of discs). This method was applied in the present and our previous studies [57, 58].

Coronary artery disease results in segmental dysfunction of the myocardium and use of imaging techniques for evaluating of regional function is a central concern in cardiac imaging. Tissue tagging is an approach unique to MRI [59]. By tracking fixed points within the myocardium over the cardiac cycle MRI tagging can address the issues of through-plane motion, in-plane translational effects, and nonouniformity of function across the thickness of ventricular wall [60].

4 CARDIAC TRIGGERING AND IMAGING SEQUENCES

Conventional MR images of the heart are degraded by complex motions of both cardiac and respiratory activity. Therefore, electrocardiographic (ECG) gating is necessary in most MRI studies of the heart to obtain diagnostic image quality. ECG gating reduces blurring in MR images caused by heartbeat or pulsating blood. The ECG signal is a record of the cumulative electrical depolarization of the myocardial cell membranes during heart activity.

An MRI-compatible ECG-sensing device is used to synchronize the phase-encoding steps in the image-data acquisition set with specific segments of the cardiac cycle. ECG gating uses the heart's electrical activity to trigger data acquisition. In ECG-gated MRI, three ECG waveform elements are important; the QRS complex, R-R interval, and T wave (Fig. 1). Gating can also be triggered by a peripheral pulse but due to the substantial delay time from the QRS complex to the onset of the peripheral pulse, ECG gating is commonly used. MRI systems also incorporate respiratory-sensing devices to reduce amount of artifacts resulting from chest wall motion [61].

ECG-triggered SE MRI is an MR technique characterized by relatively short echo times (TEs) (20-30 ms). This technique provides high tissue-to-blood contrast and is therefore well suited for detection of morphological abnormalities, but it is not fast enough to allow functional measurements.

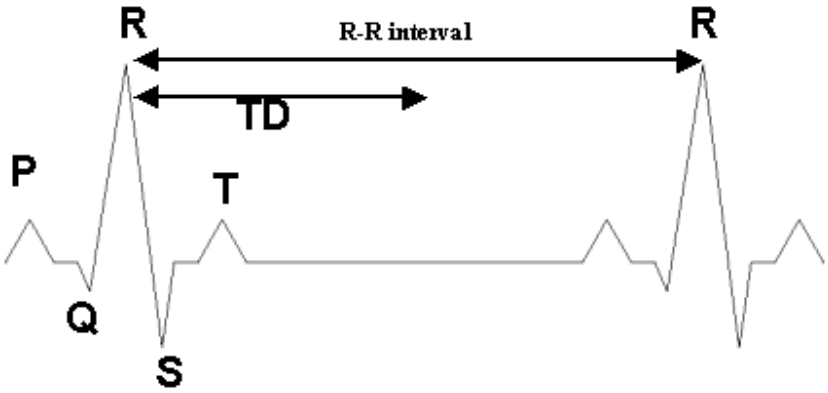

Figure 1. *ECG triggering is based on the R wave of the ECG waveform. Trigger delay (TD) defines the time from the R wave to the initiation of the imaging sequence.*

ECG-triggered GRE MRI allows the use of short repetition times (TR), short TEs, and is useful for imaging dynamic processes [62]. It is well suited for assessing ventricular function, end-diastolic volumes, end-systolic volumes, ejection fraction, and myocardial mass.

Flow velocity of blood can be measured with PC MRI, based on velocity-induced phase shifts ($\Delta\phi$) of moving protons in the presence of a magnetic field gradient (G(t)), allowing an assessment of peak velocity and volume flow.

MRI can be used for noninvasive diagnoses of heart diseases [63, 64]. In addition to anatomical cardiac imaging, MRI is capable of functional cardiac imaging, including cardiac stress testing, imaging first-pass myocardial perfusion, tagging studies, MR coronary angiography, and real-time imaging [65-70].

Two approaches to cardiac synchronization of MR acquisition have been used; 1) prospective cardiac gating or cardiac triggering was initially developed and can be used for any type of MRI sequence and 2) retrospective gating was developed for synchronization of rapid repetitive cine acquisition to the cardiac cycle [71, 72]. Retrospectively gated interpolated methods can image the entire cardiac cycle efficiently.

Detection of QRS complex is used with the prospective gating to initiate one or more sequence repetitions. In this method a phase-encoding gradient is incremented for each successive QRS complex. If TR of the sequence is very short, a complete image can be acquired within a fraction of the cardiac cycle; in this case freely selectable TD can be used to select various phases of the cardiac cycle for measurement. For extremely rapid sequences, such as echo planar imaging (EPI) and true fast imaging with steady precession (TrueFISP) several images can be acquired within a single cardiac cycle. In this case multiple slices or multiple cine frames can be acquired in a few R-R intervals.

One problem with prospective gating is cardiac arrhythmia, another problem in cardiac cine imaging is the so-called flashing artifact. A period between the last frame and the next trigger event, typically 10-15% of the R-R interval, is not sampled to allow for variations in the R-R interval and is known as arrhythmia rejection. This extra time results results in a relatively high signal level in the first cine frame due to the increased longitudinal relaxation time (T1) that occurs during the delay [71].

In retrospective gated cine acquisition images are acquired continuously while the ECG signal is recorded and subsequently sorted according to their position in the cardiac cycle [72]. This removes the flashing artifact and reduces other artifacts resulting from cardiac arrhythmia [73].

One or more slice locations, each at different phase of the cardiac cycle, can be acquired with single-phase gating (Fig. 2a). A single line of k-space is acquired for each time-phase per cardiac cycle. Utilizing the cross-R-R technique, each location is always acquired at the same phase as before in the cardiac cycle. Single-phase gating SE or GRE requires as many heartbeats as there are in-plane phase encoding lines to achieve a desired resolution (a single average). This can be used in heart studies where anatomy, not function, is being evaluated. R-R interval can be covered using the minimum possible delay between slices or evenly spaced slices within available imaging time (AIT) (Figs. 2b and 2c).

Multiphase gating allows acquisition of one or more slice locations, with each slice represented by multiple phases of cardiac cycle. The first acquisition collects the first

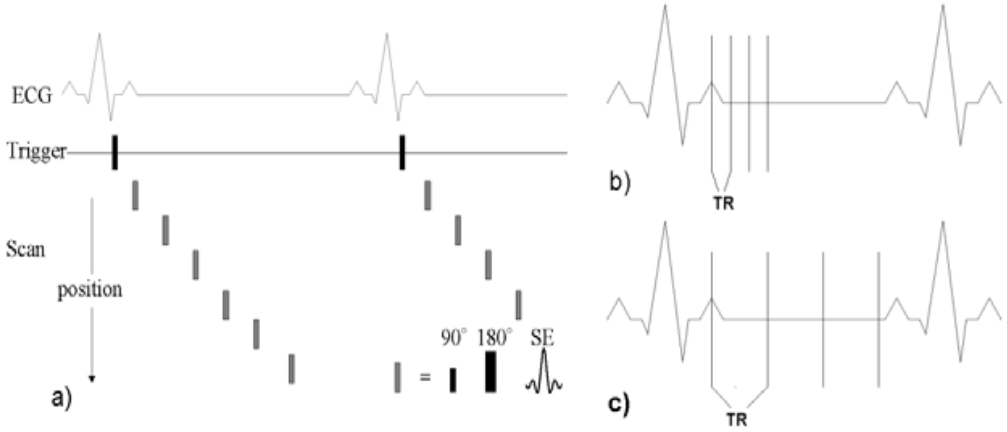

Figure 2. *a) ECG-gated SE sequence for anatomic studies, b,c) two methods of covering the R-R interval with slices using different TRs.*

slice at the first phase, the second slice at the second phase, etc. Each subsequent acquisition shifts the slice locations to a different phase, so that finally data for each phase are collected at every slice location. In cardiac MRI pulse sequences create images over hundreds of heartbeats. Thus single images in gated cine MRI is averaged across the cardiac phases.

4.1 Cardiac nonflow-sensitive techniques with MRI

4.1.1 K-space segmentation

In conventional 2-D k-space encoding, a single line of k-space is acquired per heartbeat (Fig. 3a). Each readout is accomplished in several milliseconds.

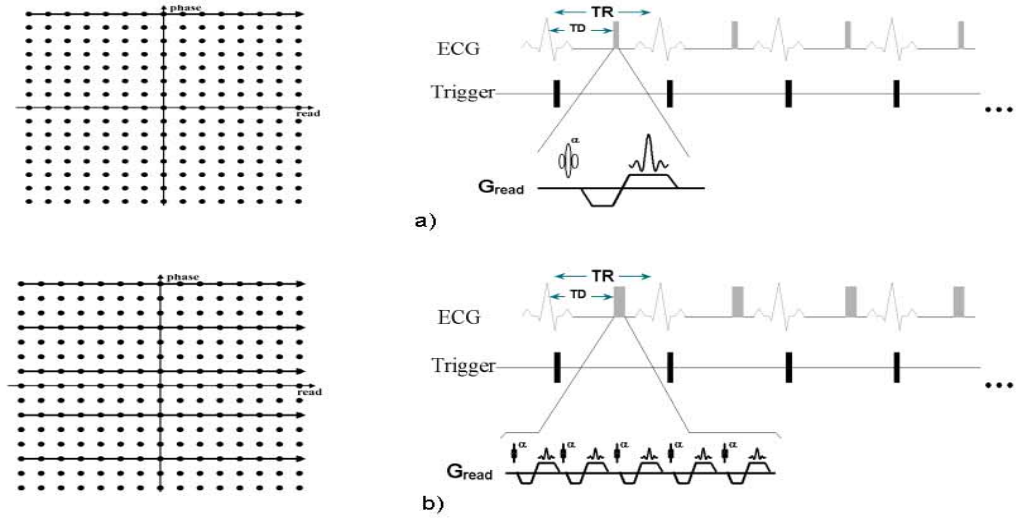

Figure 3. *a) Conventional cardiac triggered GRE, b) k-space segmentation; many phase-encoding steps are collected in a single cardiac phase. A phase-encoding gradient amplitude is changed after each excitation pulse α , TR = repetition time and TD = delay time.*

The acquisition time can be reduced by collecting multiple lines of k-space per cardiac phase (Fig. 3b). If the lines are obtained in a relatively short period, the movement of the heart does not obscure the images. With this technique, all the image data can be collected within a single breath-hold.

4.1.2 Sequences

Spin echo

The pulse sequence most commonly used for evaluating morphology of the heart and great vessels has traditionally been conventional spin echo (CSE) gated to the cardiac cycle in a multislice mode (Fig. 2a). In this technique TR is equivalent to the R-R interval. This means that imaging times in T1-weighted images are long, typically 6-8 min. The difference in contrast between the heart, epicardial fat, and the ventricular cavities is relatively good. Transverse relaxation time (T2) weighting is achieved by gating at several multiples of R-R intervals. T1- and T2-weighted images are not obtained in multiple cardiac phases, because each cardiac phase would require a separate image acquisition, e.g. 10 phases would require 10 times the total imaging time (T_S).

Volume measurements were originally performed with the CSE technique [42]. This is, however, a slow method and does not have sufficiently high enough temporal resolution [50]. In CSE presaturation slabs above and below the slices help to reduce flow artifacts. Fast spin echo (FSE) with echo train length (ETL) 8-32 for T2-weighted imaging provides shorter imaging times and better image resolution than CSE images.

Gradient echo

Traditionally, spoiled GRE imaging (FLASH = fast low-angle shot, SPGR = spoiled gradient refocuses acquisition into steady state, T1 FFE = T1 fast field echo) has been used for cine MRI of the heart. In FLASH sequences, the transverse magnetization is spoiled at the end of each of TR, thus avoiding interference of residual transverse magnetization with the next measured Fourier line [74]. FLASH has a low contrast-to-noise ratio (CNR) and relatively long acquisition times. To speed up data acquisition in FLASH, TR is shortened and bandwidth increased, but then the signal-to-noise ratio (SNR) is reduced.

In contrast to FLASH sequences, the remaining transverse magnetization is not destroyed prior to the repeated excitation pulse in steady-state GRE sequences (FISP, fast imaging with steady precession, GRASS, gradient-recalled acquisition into steady state, T2 FFE) [75].

Improvements in MR hardware have allowed new fast steady techniques such as steady state free precession (SSFP, TrueFISP) sequences [76]. TrueFISP is becoming widely available under a variety of acronyms (BFFE = balanced fast field echo, FIESTA = fast imaging employing steady-state acquisition, CBASS = completely balanced steady state). In trueFISP, the transverse magnetization is maintained between successive radio frequency (RF) pulses because the net gradient moments are zero in all three directions and no RF spoiling is implemented.

Coherent transverse magnetization continues to contribute to the signal in successive TRs, resulting in higher SNR than in magnetization-spoiled techniques such as FLASH. TrueFISP needs a very homogeneous magnetic field (B_o) because it is sensitive to off-resonance effects (banding artifacts) caused by imperfect shimming, chemical shifts, and eddy currents [77].

4.1.3 Cine gradient-echo imaging

Techniques exploiting the motion sensitivity of MRI generally fall into two categories, encoding motion either in the magnitude or phase of the magnetization. Cine imaging can be performed using a wide range of spatial resolution, temporal resolution, and scannig times.

In cardiac cine MRI, functional images of the heart are obtained throughout the entire cardiac cycle in any desired orientation. The most basic cine techniques use a flow-compensated GRE sequence synchronized to ECG [78].

The number of cine frames is dependent on TR and mean heart rate. Fig. 4 shows a diagram of a triggered FLASH sequence where N_p = the number of phases and line n

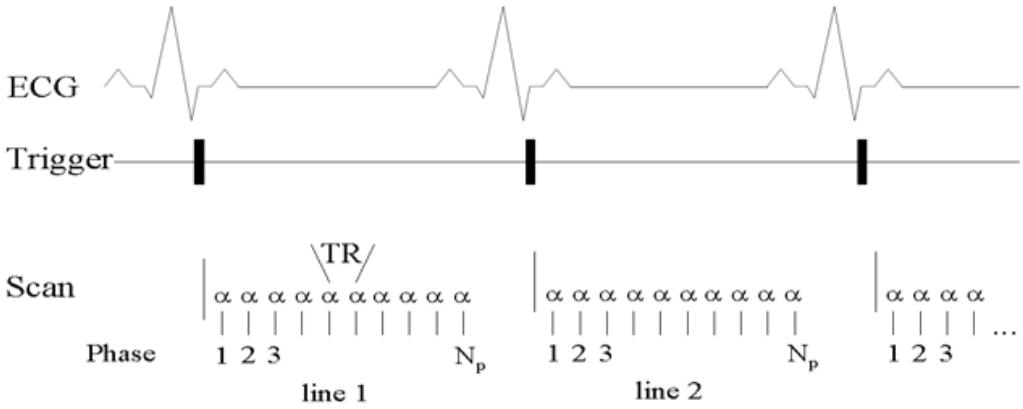

Figure 4. *Schematic diagram of single-slice prospective triggered GRE sequence. The dead time at the end of each cardiac cycle leads to increased signal intensity in the first images of the cine series. The irregularities of the heartbeat can cause significant artifacts due to degraded correlation between ECG events and cardiac motion.*

refers to the line in k-space. In conventional cine FLASH-sequence

$$N_p \times TR < R\text{-}R, \qquad (4)$$

where R-R is the mean R-R time. The total imaging time is

$$T_s = N \times N_{acq} \times R\text{-}R, \qquad (5)$$

where N = number of k-space lines and N_{acq} = number of acquisitions.

Cine GRE imaging provides rapid imaging of flowing blood with high signal intensity due to the so-called inflow effect. With conventional-type k-space encoding (Fig. 4) cine GRE has excellent temporal resolution with each readout accomplished in several milliseconds.

Segmented k-space imaging has made it possible to acquire high-quality cardiac cines in a single, typically 10-20 s breath-hold [79] (Fig. 5). The true temporal resolution in segmented k-space imaging changes, depending on how many LPS are collected. The sampling window is typically on the order of 50-150 ms. Ghosting artifacts in segmented k-space are dependent on the k-space trajectory chosen [80].

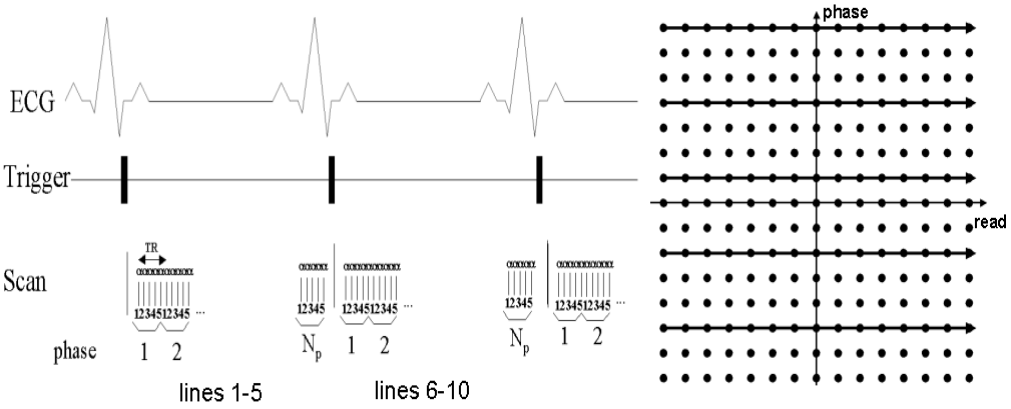

Figure 5. *Segmented k-space cine sequence with 5 lines per segment allowing complete cine acquisition of 24–35 cardiac phases in 28 s for a rate of 60 cycles/min. Using 7 lines per segment the imaging time can be reduced to 20 s with 17–25 cardiac phases.*

TR could be shortened to several milliseconds with GRE techniques such as turbo FLASH or true-FISP scanning [75, 81-83]. TrueFISP allows cine cardiac imaging even times as short as 4-8 s with a high CNR. The contrast in trueFISP is less dependent on blood flow and more dependent on the T1:T2 properties of tissue. Due to the high inherent contrast between the myocardium and ventricular cavity, and motion insensitivity, an automated segmentation process with the trueFISP sequence provides more reliable results in comparison to standard FLASH sequence [84].

4.2 Phase-contrast velocity mapping (PCVM)

Cine velocity flow mapping permits quantitative calculation of blood flow, analysis of ventricular filling patterns and valvular regurgitation, and measurement of peak velocities for estimating pressure gradients at sites of stenosis. MRI has been used to measure flow-related information, which includes anatomical mapping without the use of contrast media and velocity patterns with high spatial and temporal resolution over a wide velocity range. The major advantage of MRI for blood flow measurement is that the measurement process does not affect the flow; MRI is noninvasive and nondestructive.

Flow measurements with MRI are based on signal intensity-modulation by the inflow of fluid (TOF=time of flight), spin tagging, or flow induced $\Delta\phi$. The first effect is mostly applied to MR angiography. The tagging method can give direct visualization of slow and medium flow such as the cerebrospinal fluid (CSF) motion in the spine. The third method, the $\Delta\phi$ or PC is most commonly used for the quantification of blood flow. PCVM can be measured in a 2-D or 3-D method, but in the latter case in vivo blood-flow velocimetry is not in diagnostic use due to its inherently long scanning times.

In the presence of an applied G(t), the transverse magnetization accumulates a $\Delta\phi$ relative to spins at the null point of the G(t). This $\Delta\phi$ is a function of time r(t) and the G(t) in any of the three spatial direction with a proportionality constant c. The $\Delta\phi$ can be broken into contributions from each order of motion [85]

$$\Delta\phi = c\int r(t)G(t)$$
$$= c\int r_0\, G(t)dt \qquad \text{0. moment}$$
$$+ c\,(dr/dt)\int tG(t)dt \qquad \text{1. moment}$$
$$+ c/2!\,(d^2r/dt^2)\int t^2G(t)dt \qquad \text{2. moment}$$
$$+ c/3!\,(d^3r/dt^3)\int t^3G(t)dt \qquad \text{3. moment}$$

$$= \phi(\mathbf{r}_0,t) + \phi(\mathbf{v}_0,t) + \phi(\mathbf{a}_0,t) + \ldots, \qquad (6)$$

where $\mathbf{r}_0$, $\mathbf{v}_0$, and $\mathbf{a}_0$ are the position, velocity, and acceleration of the fluid at the start of the G(t) waveform. All stationary spins rephase at the center of a readout G(t). Higher-order contributions to the $\Delta\phi$ will not be zero at the center of readout gradient. However, this may be achieved using more lobes to the gradient waveform, to effectively null the nth order of motion at least (n+2) G(t) lobes must be used. Thus, one way to make the sequence less sensitive to higher-order motions is to use these additional G(t) lobes. TE must be increased to accommodate higher-order compensation, and thus using additional G(t) lobes is not a practical way to reduce the higher-order contributions to the $\Delta\phi$.

An alternative approach reducing $\Delta\phi$ caused by higher-order motion is to reduce the duration of the G(t) in the direction of flow [85-87]. The method is referred to as partial echo or asymmetric echo acquisition [85] .

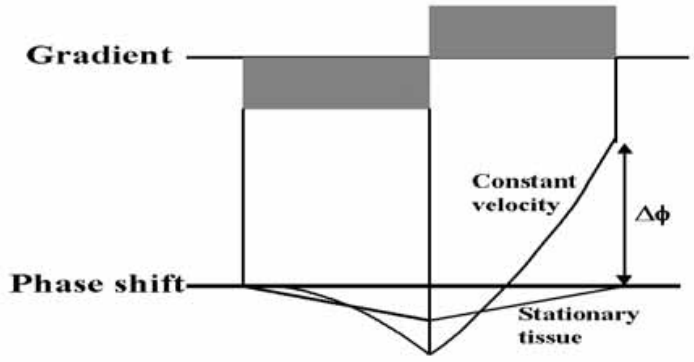

Fig 6. *Moving precessing spins experience a velocity-induced phase shift $\Delta\phi$ in the direction of the* G(t) *due to the presence of a balanced bipolar* G(t).

By applying a proper bipolar G(t) (Fig. 6), the velocity of the protons can be encoded in the phase of the received signal [9]. From Eq. (6) it can be seen that, assuming a constant velocity, the phase is described by Eq. (7) [85]

$$\phi = (\gamma\ M_1)v = \left(\gamma \int_0^{TE} G(t)tdt \right) v = (\gamma A_g T)v, \qquad (7)$$

where ϕ is the phase of the received signal, γ the magnetogyric ratio (Hz/T), ν the velocity (assumed constant), M_1 the first moment of the gradient waveform (Ts^2/m) at the echo time (TE), G(t) the magnetic field gradient (T/m), A_g the area of each lobe of the bipolar G(t) (T/ms), and T the time between the centers of the two lobes of the G(t) [9].

Early works in determining volumetric flow with MRI used a single phase measurement to calculate velocity [11, 12]. However, the simple phase image after Fourier transformation does not correspond to velocity due to inhomogeneities in the main field, motion in other directions, susceptibility variations, partial correction of the eddy current, RF effects, and pulse sequence timing may also affect phase. An almost error-free velocity map is achieved by the acquisition of a consecutive subtraction of two differently velocity encoded phase images (PCVM), since several phase errors are nearly the same for two subsequent measurements [14, 88]. In Fig. 7 two images are obtained with different values of a bipolar G(t). The first part of the sequence is flow-compensated and generates magnetization along the x-axes. The second part is flow-encoded and generates $\Delta\phi$ about angle ϕ. There are two different ways to postprocess flow images: phase difference (PD) or complex difference (CD) (Fig. 7) [89, 90]. PD subtracts the phase of two velocity-encoded images and CD takes a nonlinear arcsine function of the difference of the two images.

4.2.1 Nonsegmented PCVM

Conventional MR PCVM is performed using a GRE sequence with a bipolar velocity encoding G(t) in the desired direction of velocity measurement (Fig. 7). Conventional nonsegmented PCVM is relatively slow.

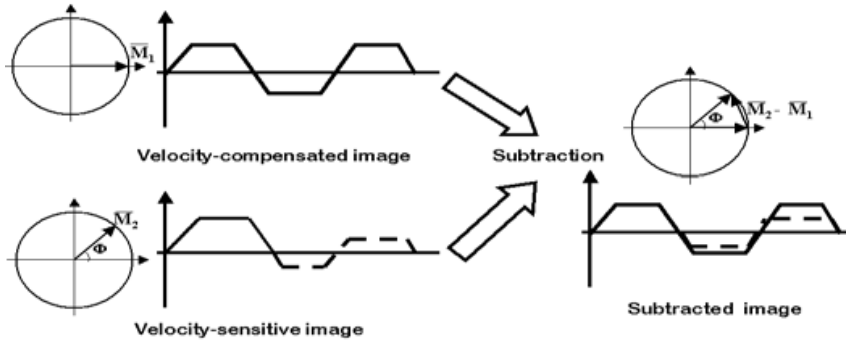

Fiqure 7. *Diagram depicting PCVM, where the complex subtraction of two datasets is obtained with different values of a so-called flow-encoded* G(t)*. The first part of the sequence is flow-compensated and the second flow-encoded.*

In MRI practice flow quantification is usually performed with 2-D PCVM [9, 12]. Cine PCVM enables voxel-based determination of flow velocities across any plane transecting the heart or great vessels [25]. PCVM measurements are well validated in vitro [91-93] and in vivo [94]. Several investigators have also measured pulsatile flow and found PCVM to be both accurate and precise [91, 95-97]. Velocity can be measured either through-plane or in-plane.

The results of the PCVM measurement can be represented with 3-D wire-frame representations at different times in the cardiac cycle. These can be used to evaluate fine flow detail, which could otherwise escape notice. The wire-frames can be viewed in a cine loop or static set.

Typical PCVM or Fourier flow technique (FFT) (Fig. 8) uses bipolar phase encoding gradients to encode the flow velocities perpendicular to the excited slice. Two measurements are acquired, the first of which is flow-sensitized and the other flow-compensated with proper G(t) waveforms. The net gradient first moment ΔM_1 is the difference in individual G(t) moments for each of the two acquisitions. Cine PCVM datasets are usually described by the velocity at which spins are given by a $\Delta\phi$ of π radians divided by ΔM_1. This velocity is referred to as the velocity-encoding value, or Venc. Thus, from these measurements a difference image of pixel-by-pixel bases is created in which the intensity of each pixel is proportional to the velocity in the encoded direction.

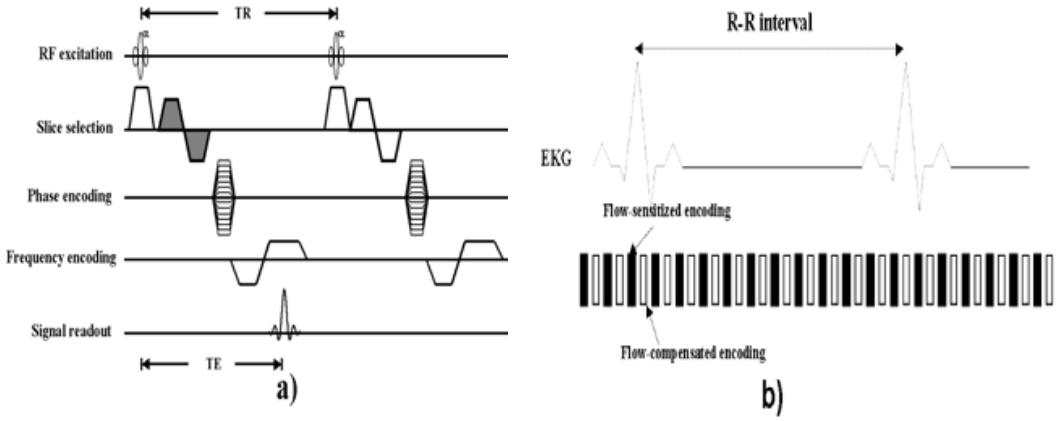

Figure 8. *a) Nonsegmented cine PCVM sequence. Flow-sensitive and flow-compensated encoding in the slice-selection direction is shown in two subsequent TR periods, b) two velocity encodings are shown interleaved within the same R-R interval.*

4.2.2 Segmented cine PCVM

Conventional nonsegmented cine PCVM is an accurate but relatively slow velocimetric technique. In this technique only one line of k-space is acquired for each time-phase per cardiac cycle, resulting in a scanning time of several minutes for acquisition of a single velocity direction in each image slice per time-phase. With the development of scanner hardware EPI sequences have been used for faster PCVM [98-101]. Total imaging time can also be reduced by acquiring a group of signals for

several phase-encoded values within a single heartbeat to be used in producing a single cine frame [79, 102-106]. This method, called k-space segmentation, has been developed to eliminate breathing artifacts by acquiring the image data within a single breath-hold.

In segmented cine PCVM multiple phase-encoded lines (=LPS) are acquired per cardiac phase. Thus scanning time is reduced by a factor equal to the LPS. This makes it possible to acquire the entire cine PCVM set in a single breath-hold period, but the number of cine frames available is then reduced.

Accurate flow results have been obtained with segmented k-space PCVM under both steady and pulsatile flow conditions (errors < 5%, using a rate of flowrates 1.7 - 200 ml/s) [106, 107]. It has also been shown to be promising in cases of moderately disturbed flow and vessel motion [103].

Various phase-reordering schemes have been suggested [108, 109]. The central portion of the k-space contributes the most contrast in the MRI image and also contains the most useful information on velocity measurements. An optimized segmentation scheme could also reduce ghosting, eddy current effects, and motion artifacts.

5 MATERIALS AND METHODS

5.1 In vitro measurements

A commercial flow phantom (UHDC, University Hospital Development Corporation, flow phantom, Quest Image Inc., London, Ontario, Canada) was applied with pulsatile flow and commercially available fluid (UHCD blood mimicking fluid, Quest Image) in the verification of flow measurements (I, III). A 5-V transistor-transistor logic (TTL) pulse generated by the flow simulator at the start of each waveform cycle was used to trigger the MRI scanner. The waveforms investigated were limited by the pump performance, however, the waveform found in the normal human carotid artery was chosen. The rigid test tube has an internal diameter of 7 mm. A 1.5-m-long rigid tube was placed upstream to the test section to ensure that flow was fully developed and undisturbed at the entrance of the model. Using the Reynolds number, we concluded that the fluid would become unstable when the mean velocity was over 71 cm/s. The flow was kept stable and uniform.

The test section was submerged in 0.1 mmol manganese chloride (MnCl) which reduced background noise and simulated the extravessel soft-tissue medium. The test section was placed in the scanner with the axis of the pipe aligned to the long axis of the magnet to avoid misalignment artifacts; either a neck coil or head coil was used (I, III). The 14 human cadaveric casts were imaged (V) and were immersed in 0.1 mmol MnCL.

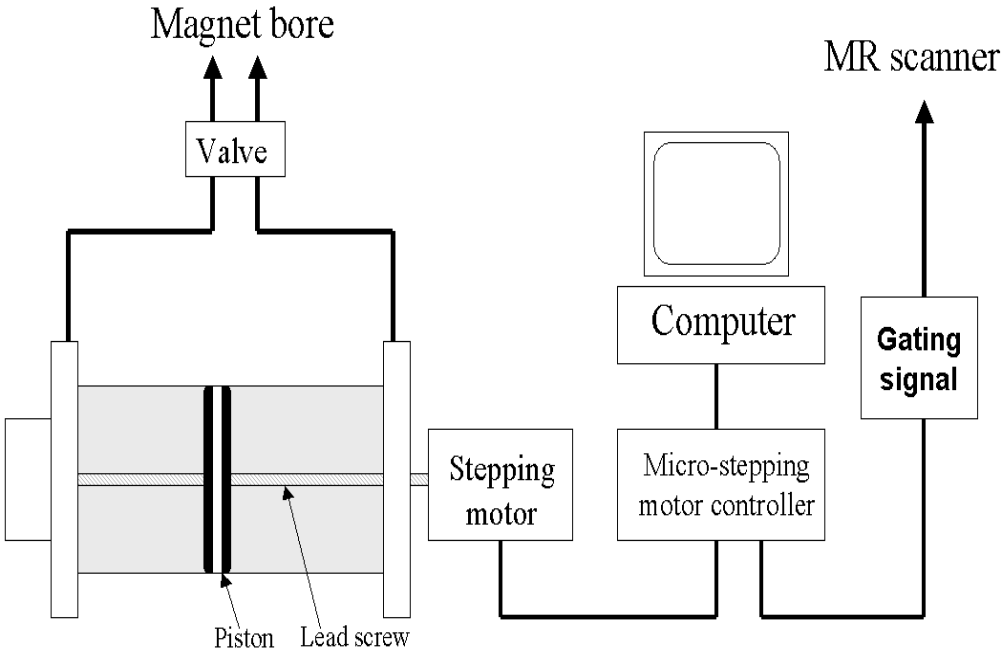

Figure 9. *Schematic diagram of the flow simulator. A computer controlled positive displacement pump can produce steady and pulsatile flow rates.*

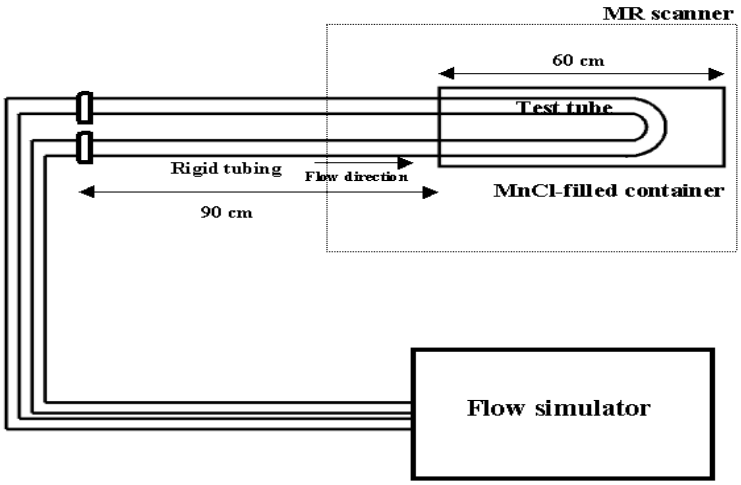

***Figure 10**. Model geometry of flow phantom. The test tube was placed in an MnCl-filled cylindrical reservoir to reduce the background noise, ensure that the neck coil received enough signal, and to simulate static body tissue.*

5.2 Subjects

Nine healthy subjects 25-56 years of age were examined in the left ventricular outflow tract study (II) and 10 healthy volunteers 26-46 years of age in the mitral flow study (III). Forty male and female patients 18-65 years of age with mild to moderate essential hypertension were studied in the aortic stiffness study (IV). Eight healthy volunteers were imaged with cardiac-gated cine MRI in the atrial study (V).

5.3 MRI methods

MRI was performed using a 1.0-T clinical MR device (II-V; Magnetom 42 SP; Siemens Medical Systems, Erlangen, Germany) or 1.5-T system (I, VI; Magnetom Vision; Siemens). The body coil was used in all human studies. The R-wave was used in ECG triggering due to its strong electrical signal. The R-R interval is the time between two successive R waves, i.e. one cardiac cycle. High-amplitude T waves could trigger the MRI system erroneously. During diastole the ventricles fill with blood; this is the period between the end of the T wave and the peak of the following R wave. The rest of the cardiac cycle is systole, i.e. the period between the R wave's peak and the end of the T wave, in which the heart is contracting and expelling blood.

The trigger window (TW) instructs the scanner when to stop acquiring data and to wait for the next R-wave trigger. During TW the system uses the time to permit the effects of the gradients to decay, thus minimizing the effect on the ECG signal. The value of TW is typically 10-20% of the R-R interval. If patients have greatly fluctuating heart rates TW value of 20-30% may be required.

TD defines the starting point after the R wave when the system can start the imaging sequence. In cardiac imaging it is favourable to start the imaging sequence (using TD) in diastole when the heart moves less than in systole. Increasing TW and/or TD reduces AIT and allows fewer slices, as does the use of fat saturation and/or magnetization transfer pulses.

5.4 MRI velocimetry techniques

The correct choice of Venc was considered critical to the quality of MRI velocity measurements, especially when the flow was assumed to be unsteady. Venc and minimal TE are often contradictory and compromising values must be used.

5.4.1 Segmented PCVM

A 1.5-T MRI system (Magnetom Vision, Siemens) capable of producing gradients of 25 mT/m with rise time of 600 μs was used. The signal was received by a receive-only neck coil and body coil was used as an RF transmitter.

The PC acquisitions were performed with flow-sensitive GRE sequence. The echo collected was asymmetric to reduce sensitivity to artifacts caused by higher-order motions. TE was 5 ms, field of view (FOV) was 100 x 200 mm^2, and the matrix size 128 x 256 pixels. The velocity sensitivity was in the slice-selection direction and the upper limit of the velocity scale (Venc) was set at 150 cm/s, which was 25% higher than the predicted peak value. The number of LPS were 1, 3, 5, 7, and 11 and the corresponding TRs were 25, 75, 125, 150, 200, and 250 ms. The cine frames were obtained every 25^{th} ms, using different TDs. The ROI used was 0.31 cm^2, which contained 50 pixels.

Table 1. Properties of the six different segmented flow sequences

Phase-encoding lines/segment	Pixel sizes (mm^2)	TR (ms)	Acquistion time window (ms)	Cardiac cycles needed	No. of sequence repetition
1	0.77*0.78	25	25	131	1
3	0.79*0.78	75	63	42	3
5	0.77*0.78	125	105	26	5
7	0.79*0.78	150	147	18	6
9	0.79*0.78	200	189	14	8
11	0.79*0.78	250	231	12	10

Table 1. *Properties of the sequences used in segmented k-space flow study. TR was chosen to be such that cine frames were obtained every 25th ms in every sequences. The true temporal resolution i.e. data acquisition window chances when lines/segment are increased.*

The size of the data-acquisition windows, as is the true temporal resolution, is dependent on how many LPS were collected. The number of phases available in the cardiac cycle is RR/mxnxTR, where RR is the R-R interval, m the number of flow encodings in the sequence and n the number of LPS collected.

K-space segmentation scheme

Two possible phase-encoding ordering schemes with LPS 7 are shown in Figs. 11 and 12. In the conventional sequential scheme (Fig. 11) the central phase-encoding lines 56 – 63 and 64 – 70 (central lines 63 and 64 are usually acquired at those times during which they show the greatest possible temporal difference) with most of the signal power are acquired at different phases of the cardiac cycle. This method tends to suffer from significant blurring and ghosting artifacts, which increases with greater

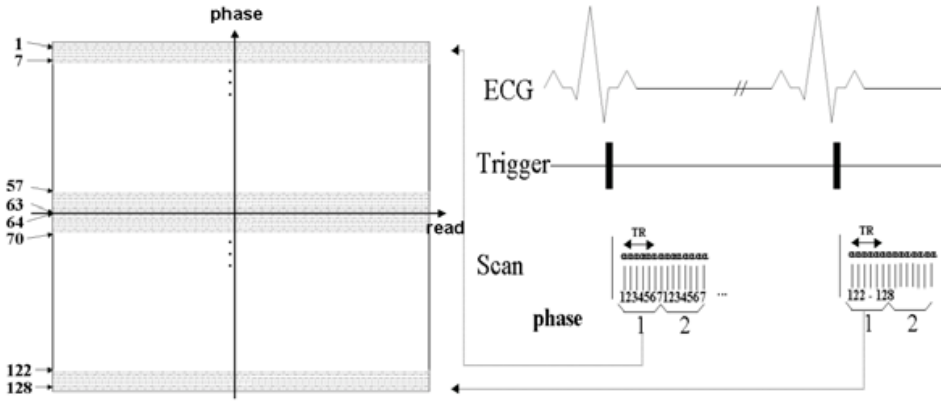

Figure 11. *Depiction of conventional sequential-segmented k-space method with LPS 7. Two central lines, number 63 and 64, are acquired with greatest possible temporal difference.*

number of LPS. In this study introduced segmented scheme (Fig. 12), the k-space was divided into 7 segments, and during each cardiac cycle for each cine frame one line from each segment is acquired (I). In this approach the entire k-space is traversed in each segment and central lines 59-73 were acquired at the same time period, thus reducing the nonuniform modulation of low spatial frequency.

In this type of k-space scheme the number of central k_y lines is the same as the number of segments, and the most central part of the k-space is acquired at the same time as the cardiac cycle. The central portion of the k-space contributes most of the contrast in the MRI image and also predominates in the velocity measurements.

Acquiring the echo asymmetrically within the data-acquisition period minimized the duration of velocity encoding G(t). The peak of the echo occurred at data point 82 out of 256 and the missing data points were zero-filled. The Venc was 150 cm/s.

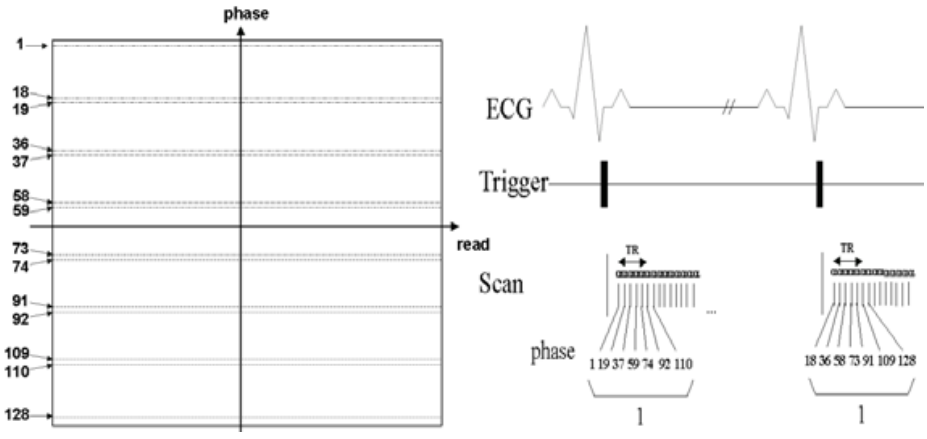

Figure 12. *Depiction of new segmented k-space method with LPS 7. The central lines 59-73 are acquired at the same time period.*

In segmented PCVM with N k-space lines per segment, the most useful information is contained in the central line of the segment, (N+1)/2, because this is the closest line of the segment to the center of the k-space. Therefore, the time point corresponding to each cardiac phase was adjusted to be the time of acquisition of the central k-space line of the segment. As a result, segmented techniques cannot acquire data at the very beginning of the cardiac cycle. This may result in uncertainties in measurements for patients with very rapid, early systolic flow acceleration. Use of retrospective ECG gating should eliminate this problem.

The segmented scheme with LPS 5 would generally require more than 20 s per acquisition, which is too long breath-hold period for many patients. Increasing the number of k-space lines per segment will shorten the acquisition time, but at the expense of temporal resolution. The data-acquisition window can be obtained with the equation

$$\text{data-acquisition window} = m * n * TR, \qquad (8)$$

where m is the number of flow-encodings (in this study m = 2), n the number of phase-encoding steps (LPS) acquired for each cardiac phase within each heartbeat and TR the repetition time of the sequence.

5.4.2 Image analysis

Both the magnitude and phase images were reconstructed for each image dataset from the cine acquisition. The magnitude image was used to aid in drawing the ROI. The mean $\Delta\phi$ was measured in the ROI adjacent to the tube. The background correction was made by subtracting the mean velocity in the ROI from the mean phase in the background area. The mean flow values were calculated from the background-corrected mean phase values by using information of the velocity-phase relationship. Volume flow was calculated by multiplication of the mean velocity and vessel area. Linear phase correction, which reduces low-frequency phase variation, was performed automatically in both flow-compensated and flow-sensitive images.

5.4.3 Velocity profiles

The results of the PCVM measurement can be represented with 3-D wire-frame representations at different times in the cardiac cycle (II, III). These can be used to evaluate fine flow detail. The wire-frames can be viewed in a cine loop, or static set.

Spatially complete cross-sectional velocity maps could not be produced with the ultrasound method. Velocity encoded cine MRI enables noninvasive determination of flow profiles across any section of the heart or great vessels [25]. The velocity encoded phase images show the velocity of the spins in each individual voxel of the image in the velocity encoding direction.

Assumption of the spatial homogeneity of cross-sectional left ventricular and mitral flow is fundamental in Doppler ultrasonography when measuring stroke volume and aortic valve area [110, 111]. The in-plane spatial resolution (~ 1-3 mmxmm) was sufficient to obtain details of the velocity profiles for a large vessel such as the

ascending aorta. Higher spatial resolution would resolve the velocity gradients immediately adjacent to the vessel wall.

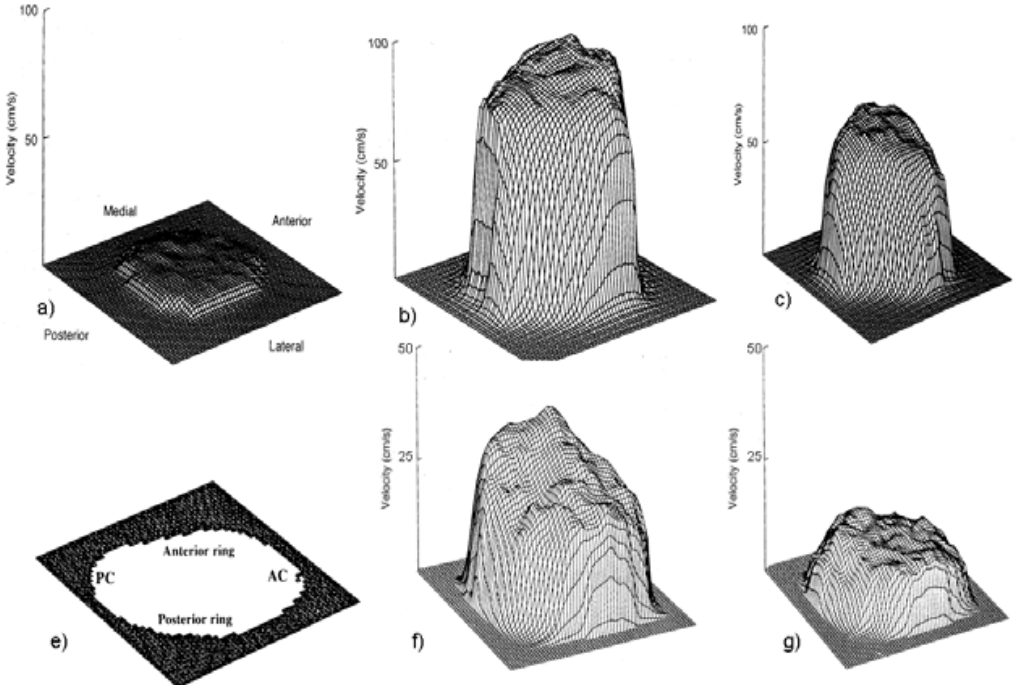

Figure 13. *Five images of a series of 3-D blood flow velocity profile plots representing the instantaneous flow-velocity distribution across the left ventricular outflow tract (a, b and c) and mitral annulus (f and g). The orientations of the views are shown in a) (left ventricular outflow tract) and in e) (mitral annulus), in which a) represents the early phase of ejection and b) midsystole at the time of peak flow across the left ventricular outflow, f) represents the early diastolic rapid-filling period, and g) the late diastolic filling period. The instantaneous blood-flow rate can be calculated by integrating of the velocity profiles over the lumen of the vessel.*

Left ventricular outflow tract and mitral flow profiles (II, III)

Imaging technique

Multislice T1-weighted SE coronal slices were obtained to localize the aortic root and left ventricular apex (II). Another series of 8 parallel oblique SE images were acquired to image the left ventricular outflow tract during systole. One midsystole SE image was selected, and PC image plane was placed 0.5-1.0 cm below the level of the aortic annulus. The velocity encoding was performed in the slice-selection direction, which means that velocity was encoded parallel to the longitudinal axis of the outflow tract. FOV was 350 mm x 350 mm and the matrix size 192 x 256 pixels, resulting in pixel dimensions of 1.8 x 1.4 mm; the section thickness was 6 mm. TE

was 6 ms and TR 30-40 ms. The upper limit of the velocity scale was set at 150 cm/s.

After acquiring the coronal localizing series in the mitral flow study (III) to identify the aortic root and left apex, a long-axis cine series of the left ventricle and left atrium, consisting of 6-8 contiguous 10-mm slices, was obtained. These cine studies were used to set the image plane for the PCVM examination of mitral transannular flow. The sequence showed velocity sensitivity in the slice direction and because TE was chosen to be 6 ms, $\Delta\phi$ values caused by higher orders of motion could be minimized. FOV was 350 mm x 350 mm and the matrix size 192 x 256 pixels; the section thickness was 6-8 mm. TR 30-43 ms depending on the heart rate. The upper limit of the velocity scale was set at 120 cm/s.

The validity and reproducibility of the flow measurements were tested with a commercially available flow simulator (UHDC computer-controlled flow simulator, Quest Image) and blood-mimicking fluid (Quest Image). Steady flow at rates of 5, 10, 15, 20, 25 and 30 ml/s in a tube was produced.

Image analysis

To quantify regional differences in spatial flow systolic velocity in the left ventricular outflow tract time curves were reconstructed in 9 different areas (II). Each ROI was a circle encompassing an area of 0.2 cm^2 (8 pixels); these circles were placed manually over the PC image frame-by-frame, one in the center of the outflow tract and the rest peripherally in 8 sectors 45^o to the flow area. The regional instantaneous velocities were calculated as means of the pixels included in each ROI. Regional velocity-time curves covering the entire systole were reconstructed by plotting the velocity at each phase against the delay of the phase from the R wave. The regional mean systolic volumetric flow rate was calculated as a product of the temporal mean systolic velocity and the known size of the flow area. The spatial mean velocities were analyzed similarly, but using the ROI surrounding the entire subaortic annulus.

To measure differences in spatial velocity in the mitral annulus (III), 5 different areas were acquired with PC sequence. Each ROI was a circle comprising 28 pixels (0.6 cm^2). They were positioned manually over the PC image, one centrally and the rest anteriorly and posteriorly and in the two opposite commissural areas of the annulus. To determine the early diastolic velocity peaks the ROIs were defined on a PC image coinciding with the most rapid early flow. The measurements of mid- and late diastolic velocities as well as the reconstruction of the regional velocity-time curve were based on a late diastolic PCVM image. The velocity at each phase as well as mean volumetric flow rates were determined as above in the left ventricular outflow tract (II). The possible spatially dependent phase offsets were corrected in all velocity measurements, using a circular background region (area = 2.4 cm^2) in the periphery of the liver.

Repeated measures-analysis of variance was used to assess whether there were statistically significant overall differences in velocity recorded in the different regions. If the F-value was significant, selected pairwise comparisons were made with Student's paired t test. Bivariate correlation coefficients were calculated with the Pearson's product method. The calculations were performed on the personal

computer using commercially available software (SYSTAT^{TM} version 5.1, Systat Inc., Evanston, IL, USA).

5.4.4 Aortic pulse wave velocity

The FWV in the thoracic aorta was chosen as an index of aortic stiffness. To determine the FWV, velocity-sensitive cine images were acquired at the height of the pulmonary bifurcation in the ascending aorta and distally close to the diaphragm in the descending aorta. The velocities were encoded perpendicular to the aortic cross-sections, using a double-oblique image. The sequence used interleaved acquisition of flow-compensated and flow-sensitive GRE signals with TR of 30-40 ms, depending on the heart rate, and TE of 6 ms; FOV was 350 x 350 mm, slice thickness 8 mm and the upper limit of the velocity scale (Venc) 120 cm/s.

The data were used to reconstruct velocity-time curves separately for the cross sections of the ascending and descending thoracic aorta. The foot-to-foot flow wave transmission time was measured by estimating from the intersections of the linear extrapolation of the early systolic slope. The late diastolic flow was used as a baseline. The distance between the aortic cross-sections is determined in an oblique sagittal image of the thoracic aorta by tracing a cursor along the center of the lumen. The FWV was calculated in meters per second as the distance divided by the transmission time.

5.5 Assessment of aortic distensibility and cardiac volumetry

5.5.1 Aortic distensibility

The effects on aortic stiffness of antihypertensive treatment were determined (using two different drugs) (IV). The studies were performed using a 1.0 T superconductive scanner (Siemens), a body coil, and ECG triggering.

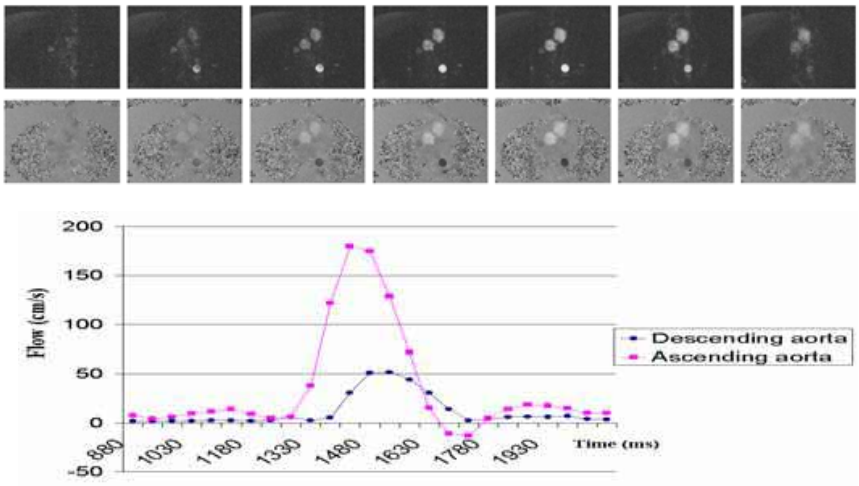

Figure 14. a*) Seven phase and modulus images of a cine PCVM series through the chest. The descending aorta is depicted in darker shades and the ascending aorta as brighter shades of gray. b) Flow versus time curve for the ascending and descending aorta was obtained from analysis of the cine PC- study.*

A cine-examination was acquired in a plane transecting the ascending and descending thoracic aorta at the level of pulmonary artery bifurcation. A 2-D GRE sequence with a TR of 50 ms, TE of 12 ms; flip angle (FA) of 30°, imaging matrix 128x256 pixels, and slice thickness 7 mm were used (IV).

The MR images were analyzed in an off-line image analysis system (Radgop/wiz, Contextvision, Struers Vision AB, Linköping, Sweden). The smallest and largest circumferences of the ascending and descending thoracic aorta were selected from the cine series. The change in aortic luminal area from end-diastolic to end-systole was calculated. Aortic strain was determined as the change of the aortic luminal area from its diastolic minimum to its systolic maximum divided by the systolic area. Peterson's aortic E_p (pulse pressure/areal strain) was also calculated.

5.5.2 Atrial size and function

MRI was used to determine the volumes of the right and left atrial casts and to assess right atrial volume cycles in healthy subjects. The left ventricular cavity volume was also imaged.

The casts were embedded in a 0.1 mM MnCl solution. The cine sequence used in the in vivo studies produced artifacts around the cast, necessitating the use of T1-weighted SE sequences with the following parameters: TR 350 – 450 ms, TE 15 ms; FOV 230 mm x 230 mm; matrix size 256 x 256 pixels; and slice thickness 10 mm. The volume of the casts was calculated using the method of discs. The true volume of each cast was measured with the water-displacement method. The reproducibility was tested by measuring the right atrial casts twice in double-blind studies.

The right atrial volumes of 8 healthy adult volunteers were determined. A GRE sequence (FISP) with FOV of 340 x 340 cm, TR 25 ms, TE 12 ms, imaging matrix 128 x 256 pixels, slice thickness 10 mm, FA 30° for the atrial and 60° for the ventricular studies were used. Two nonadjoining 10-mm-thick slices were acquired simultaneously, leading to effective phase duration of 50 ms.

The images were analyzed in an off-line image analysis system (Radgop/wiz, Contextvision; Struers Vision) connected via the Ethernet network to the MRI console. After the data set was transferred, the area of each slice was planimetered using a mouse-driven cursor, and the 3-D volumes were reconstructed by summing up those 2-D images with a thickness of 10 mm (the method of discs). 6-12 contiguous long-axis slices encompassed the entire atrial cavity. The cavity volumes at each 50-ms phase were reconstructed. The right atrial volume-time curves were illustrated by plotting each instantaneous atrial volume against time after the R wave of the ECG at which the acquisition was performed. The atrial maximum and minimum volumes were determined from the volume-time curve, and their difference was taken as the cyclic volume change. The calculated right and left volume curves were compared.

5.5.3 Right ventricle size

The study was performed using a 1.5-T imager (Magnetom Vision, Siemens). A GRE sequence (FLASH) was used to image the human 4-chamber cadaveric casts. The

actual cast volumes were measured with the water-displacement technique. The images were analyzed with a Siemens console using Siemens application software (Numaris VB31B).

6 RESULTS

IN VITRO STUDIES

Flow phantom

Precision of fast magnetic resonance velocity mapping (I)

The precision of flow measurement in breath-hold, segmented k-space flow sequences was evaluated using a flow phantom. The first three steady flows (10, 20, and 25 ml/s) were evaluated using LPS 1, 3, 5, 7, 9, and 11. The calculated theoretical mean velocities were 31, 62, and 78 cm/s. The mean velocities were drawn as a function of LPS and the corresponding regression lines were: v_{mean} = -0.07 x LPS + 30.3 , v_{mean} = -0.42 x LPS + 59.7, v_{mean} = -0.94 x LPS + 75.2. The mean velocity (v_{mean}) in the center of mass of the pulsatile peak is a constant (v_{mean} = 40.1 ± 2.9 cm/s) and time T = -10.1 x LPS + 268 (r = 0.9937, P < 0.0001). The correlation between theoretical and experimental flow curves is also linear as a function of LPS: C = -0.9796 x LPS (r = 0.9873, P < 0.0001).

IN VIVO STUDIES

Left ventricular outflow and mitral annulus flow-velocity profiles (II, III)

The velocity encoded MRI images were acquired to measure flow through the left ventricular outflow tract and mitral annulus in normal humans. The idea of spatial homogeneity of flow was questioned by the results of measurement of systolic flow velocities in the left ventricular outflow tracts and by the creation of cross sectional flow profiles.

Cross-sectional flow maps in the left ventricular outflow tract in healthy volunteers showed nonuniform velocity profiles. The most rapid flow was through the anterior-medial sector of the flow area. The nonuniformity was most conspicuous at the time of peak systolic flow. The spatial inhomogeneity of the peak velocity, calculated as the percentage ratio of the range of the regional measurements about their mean, averaged 18.2 ± 5.0%, and the inhomogeneity of the mean flow rate was 19.2% ± 3.5%.

The mitral annulus flow shows marked spatial inhomogeneity in normal humans; the individual spatial inhomogeneity averaged 33.5 ± 13.8% for early velocity peak (range 14.3-56.2%), 41.1 ± 16.1% for the late diastolic velocity peak (range 10.5-60.0%), and 70.0 ± 33.9% for the mean diastolic flow rate (range 11.0-147.1%). The individual percentages of regional inhomogeneity were unrelated to heart rate.

Assessment of aortic distensibility (IV)

The effects of 6 months of treatment with an angiotensin-converting enzyme (ACE) inhibitor (cilazapril) or a [beta]1-adrenergic blocker (atenolol) on aortic stiffness in essential hypertension was assessed. The aortic E_ρ was determined with cine MRI and indirect brachial artery blood pressure measurements prior to and after three

	Baseline	3 weeks	6 months
FWV (Cilazapril) (m/s)	8.8 ± 3.8	7.7 ± 2.7	7.5 ± 1.7
FWV (Atenolol) (m/s)	7.7 ± 3.8	8.2 ± 2.1	7.0 ± 2.1
E_ρ (Cilazapril) (Pa)	1053 (643 –1459)	811 (635-1124)	821 (465-1770)
E_ρ (Atenolol) (Pa)	790 (560-1668)	944 (650-1382)	1077(736-1772)

Table 2. *Effects of cilazapril and atenolol on the aortic flow-wave velocity (FWV) and the stiffness (E_ρ) of the descending thoracic aorta*.

weeks and 6 months of therapy. The reductions in systolic and diastolic blood pressures from baseline to 6 months averaged -17 ± 13 and -10 ± 6 mmHg, respectively, with cilazapril and -23 ± 16 and -14 ± 6 mmHg with atenolol. Concomitantly, the E_ρ of the ascending aorta decreased with cilazapril from a median of 2.234 x 10^2 Pa (2.234 x 10^3 dyn/cm^2) (interquartile range 86.6 - 374) to 0.868 x 10^2 Pa (0.868 x 10^3 dyn/cm^2) (51.5 - 148.6) and with atenolol from a median of 1.611 x 10^2 Pa (1.611 x 10^3 dyn/cm^3) (89.5 - 279) to 1.054 x 10^2 Pa (1.054 x1 0^3dyn/cm^2) (61.6 - 186). In repeated-measurements-analysis of variance, the change in E_ρ with time was statistically significant ($P < 0.001$) but the group - time interaction was not. The FWV was reduced (Table 2) with antihypertensive treatment, but the changes were not statistically significant.

Right and left atrial casts (V)

A series of 14 cadaveric human right atrial casts was studied. The volumes of the right atrial casts (64-187 ml) correlated closely ($R = .99$, $P < .001$) with the true volumes (70-206 ml). A small underestimation was found (-7.2 ± 2.3 ml, $P<0.01$). The 14 human left atrial casts ranging from 19 ml to 119 ml correlated well with the true volumes varying from 19 ml to 113 ml. A very small underestimation was again observed (-1.7 ± 2.1 ml, $P = 0.009$).

Right atrial volumes and volumetric function in healthy subjects (V)

The maximum right atrial volume averaged 148 ± 26 ml and minimum 72 ± 18 ml. The minimum, maximum, reservoir, and stroke volumes were larger and ejection fraction smaller in the right atrium than in the left atrium.

Right ventricle casts (VI)

There were no statistically significant differences between the measured and true right ventricular volumes. The axial plane gave the smallest mean absolute differences from the true ventricular volume (3.2 ± 2.2 ml) and also best repeatability of volume analysis (0.2 ± 1.6 ml).

7 DISCUSSION

The present study shows that both conventional and segmented k-space cine MRI PCVM are methods accurate enough for use in in vitro and in vivo studies. MRI PCVM has been applied successfully in the aortic outflow tract and in determination of mitral flow and aortic FWV. Nonvelocity-sensitive cine MRI has been applied in cardiac volumetric studies. The validity and repeatability of volume measurements in cadaveric casts and healthy volunteers were favourable.

7.1 ECG gating

To completely cover the diastolic part of the R-R interval, oversampling into the next cardiac cycle was used; thus the phases were selected to exceed the cardiac cycle by a factor of 2 – 4 (III, V). The entire cycle was then covered, but the scanning time was greatly lengthened and the variation in cardiac rate could temporally blur the late frames. A retrospective gating strategy acquires data at the constant rate and data is linearly interpolated into the closest temporal phase.

Only prospective gating was available in this study. Environmental artifacts resulting from the B_0, RF pulses and gradient fields distorted the ECG waveform. These could cause triggering to occur from any wave that is not the R wave resulting in corruption of entire cine series. The electrodes and cables were placed carefully to minimize the tradeoffs to ECG waveforms. MR-compatible monitoring equipment provided by the scanner manufacturer was used in order to ensure that the monitoring devices fulfilled the standards for diagnostic ECG equipment in the MR environment. Arrhythmias can result in a poorly defined QRS complex, which generally does not allow for adequate ECG gating and thus results in a poor examination. In our studies none of the healthy volunteers or patients had extra ventricular systoles.

Using retrospective ECG-gated cardiac examination could have resulted in benefits such as a) less systematic noise and blurring, b) avoidance of lighting artifacts, c) representation of the entire cardiac cycle, and d) less sensitivity to artifacts resulting from irregular heart rates. However, the quality of the ECG is extremely important in retrospective gating.

The T-waves appeared with higher amplitude inside the magnet than outside. The so-called magnetohydrodynamic effect has a detrimental effect on ECG and causes signicant artifacts over T-waves. The effect is most pronounced at high blood velocities (systole). The changing G(t) induces electromagnetic fields into the loop of ECG signal leads, which appeared as noise (I, II and IV). When the studies were focused on the diastolic events of the cardiac cycle, the artifacts caused by the magnetohydrodynamic effect were not as eminent.

To avoid superimposition of the ECG signal by electrical voltages induced in B_0 by thoracic motion, RF pulses and switching gradient fields the ECG can either be converted to an optical signal and carried out along a fiberoptic cable or transmitted by radiotelemetry at a frequency that does not interfere with the MR signal [112, 113]. The vectorcardiogram (VCG) from multiple ECG channels also improves QRS

detection accuracy [114]. Any trial-and-error iteration to find a suitable ECG form can be avoided using VCG-gated MR-acquisition, thus, the patient setup time is reduced. A new ”self-gated" acquisition technique extracts the motion synchronization signal directly from the same MR signals used for image reconstruction and thus eliminates the need for ECG gating in cine MRI [115].

7.2 MRI

All the human and right ventricular cast studies were performed with a body coil, while a neck coil and a head coil were used in flow phantom and atrial cast studies; only 2-D sequences were used. The voxel size was kept rather large and a rectangular matrix was generally used to improve the SNR and reduce the imaging times (fewer phase-encoding steps). Pixel size varied from 1,8 x 1,3 mm^2 to 2,9 x 1,4 mm^2 when body coil was used and 0,78 x 0,78 mm^2 to 0,90 x 0,90 mm^2 with the head and neck coil setup. The slice thickness ranged from 6 to 10 mm.

Respiration also results in some image artifacts. These can be reduced by synchronizing data acquisition to both the cardiac cycle and respiration [116]. In the present study respiratory gating was not used because it was very time-consuming. The detrimental effect of breathing can also be reduced by selecting phase-encoding direction in head-to-feet direction and using saturation bands. Fast-imaging techniques, such as segmented k-space acquisition and high speed imaging can also reduce problems associated with respiration. Breath-hold k-space segmented cine MRI has been shown to be accurate for evaluation of cardiac function and anatomy [117].

7.2.1 Imaging sequences

Our first cine studies were performed with FISP sequence. Due to its relatively long TR the contrast was similar that of FLASH sequence. In a moving heart, true steady-state contrast can not be expected with FISP sequence. FISP was replaced by FLASH sequence, because FLASH made it possible to use k-space segmentation. Recently improvement in MRI scanner hardware has made it possible to implement cine examination using TrueFISP or BFFE which has balanced, rewinding gradients in all three directions. TrueFISP requires good shimming and high-performance gradient technology to obtain very short TEs.

Gradient echo (FLASH) sequence was used in flow-sensitive cine examinations. Volumetric studies were performed both with a cine steady-state sequence (FISP) and FLASH sequence. In pilot studies SE sequence was also applied to measure cardiac volumes. However, GRE sequence gave the best definition of blood flow from the myocardial border. Velocity compensation was used in the slice-selection direction only in GRE sequences, which added contrast and reduced some blurring in the image. A more pronounced effect on image sharpness would have been achieved by also using velocity compensation in the read direction. However, this increases TE and TR, which we tried to keep short to avoid velocity-induced phase dispersion. Short TRs were necessary to obtain additional cine phases. Signal loss from abnormal flow patterns is dependent on the rephasing properties of the imaging sequence and also on whether the major flow component is along the read or slice-

selection direction. It was not feasible to apply higher-order motion compensation in the MRI system used in this study, which would have increased TE and TR even more.

In GRE imaging, contrast is strongly dependent on the FA. In flow-sensitive cine studies (I-IV) FA was 30^o. In the atrial study FA was 30^o for human atria and 60^o for the human ventricle (V). The FA of 25^o was chosen for the ventricular cast study (VI). Blood flow through the imaging slice does not attain equilibrium, which is expected to result in a brighter image with an increasing flip angle. However, the blood signal intensity has high directional dependency at high FAs and leads to heterogeneous signal distribution in the blood pool; therefore the FA was kept rather small. In multislice acquisition, small gaps between the slices also decreased the signal intensity of blood flowing to the ventricle due to the saturation effect. This also led to a more uniform blood signal.

Siemens Magnetom SP42 magnet did not have shielded gradients, and eddy currents introduced spatially dependent offsets in the flow values observed (II-V). In the newer system (Siemens Magnetom Vision), eddy current effects were largely eliminated by shielded gradients (I, VI).

7.2.2 Velocity-sensitive cine imaging

All the flow-sensitive sequences used were based on triggered 2-D PC sequence (FLASH). Nontriggered 2-D PC sequence has also been applied successfully when flow is moderately pulsatile [118].

In the preliminary PCVM studies, FLASH sequence with one velocity-compensated part at the beginning and a velocity sensitive part in other phases of the cardiac cycle was used. In the final data the same velocity-compensated image was subtracted from the velocity-sensitive images. In this method the data acquisition window was short, but the method suffered from many artifacts and inaccuracy. By changing the sequence to an interleaved method, the number of cine frames and the temporal resolution of the cine data were reduced by about a factor of two. This, however, minimized view-to-view misregistration and errors arising from magnetic susceptibility differences, B_0 inhomogeneities, and eddy currents.

The accuracy of interleaved PCVM has been found to be high, with an error less than 10% even in relatively complex flow patterns [119]. The flow measurement accuracy of GRE-based segmented PCVM sequences in a phantom mimicking heart motion during acquisition has been also evaluated [120], in which segmented sequences also gave accurate results. All the flow measurements in this study involved pulsatile flow both in vivo and in vitro.

PD subtraction was used in some studies (II-IV) and CD subtraction in another (I). When the voxels in the lumen contain both flowing spins and stationary tissue, substantial error is introduced in the calculated flow values. The error is proportional to the relative number of edge voxels. The proportion of partially occupied voxels, in turn, is determined by FOV, matrix size, slice thickness, and angle between the imaging slice and flow direction. In the present human MRI studies quite large FOVs and large pixel sizes were used. Especially low resolution shows a tendency to

overestimate the flowrate, due to the partial-volume effect. The use of CD subtraction in flow measurements has greater immunity to partial-volume effects than the PD method [90]. This makes CD subtraction especially useful for flow measurements obtained for small-diameter blood vessels. The use of large FOVs without corresponding increase in errors due to partial-volume effects is possible by applying the CD subtraction method.

7.2.2.1 Sources of error in cine PCVM

Errors in PCVM measurements can be classified as systematic or random. Flow-related artifacts are essentially caused by an asymmetrical Fourier transform, which is described by the following equations.

The standard Fourier transform can be written as

$$H_0(f) = \int f_0(t) e^{j2\pi ft} dt \tag{9}$$

$$f_0(t) = \int H_0(f) e^{-j2\pi ft} df \tag{10}$$

By introducing an error function $e^{jg(t,f)}$, the Fourier transform pair is modified as

$$H(f) = \int f_0(t) e^{j2\pi ft} e^{g(t,f)} dt = e^{jg(t,f)} \cdot H_0(f) \tag{11}$$

$$f(t) = \int H(f) e^{-j2\pi ft} df = e^{j\Phi(t)} \otimes f_0(t) \tag{12}$$

Depending to how complicated the error function is, the original function can be shifted, blurred or distorted. To suppress these artifacts the imaging sequence must be optimized, which implies that shortest TE and proper and efficient gradient waveforms should be used.

7.2.2.1.1 Accuracy

The PC technique has been validated and proven to be a robust method with high accuracy in measuring flow [89, 121]. However, limiting artifacts do occur.

Partial-volume effects

Partial-volume effects in flow measurement mean that some of the voxels that cover the vessel lumen contain both flowing blood and stationary tissue. The resultant error is caused by spatial undersampling of velocity distribution and is proportional to the relative number of edge voxels. The accuracy of flow measurements decreases with increasing slice thickness [89]. It has been suggested to increase the spatial resolution so that the lumen contains at least 16 pixels to keep the error within 10% [122].

Using small FAs and short TEs, the difference in signal magnitude between flowing blood and the surrounding stationary tissue can be minimized and thus the partial-volume effects reduced [122]. Larger voxel sizes and thus increase in the proportion

of partially occupied voxels results in higher values in flow measurements [97]. Acquisition parameters such as slice inclination, slice thickness, and flip angle affect the magnitude of the partial-volume effect, but the impact of these parameters on accuracy of flow measurement is relatively small [97]. Partial-volume effects become more significant in locations with large velocity gradients.

Intravoxel phase dispersion

The use of 2-D PCVM assumes symmetrical distribution of the velocity phase within a voxel. The fluctuating velocities corrupt the phase of the magnetization. The resultant intravoxel phase dispersion causes asymmetry, which can be minimized by increasing spatial resolution, shortening TE, and decreasing the velocity sensitivity of the experiment [123]. The signal will be completely lost when the spread of the phases within a volume is of the order of π radians.

Phase offsets

Theoretically, the phase in voxels within stationary tissue should be zero, but phase errors may introduce spatially dependent offsets ($\Delta\phi$) in the observed flow values. Eddy currents, improperly balanced gradients, susceptibility, or inhomogeneity of main magnet field may cause these offsets. These $\Delta\phi$ effects can cause significant errors when quantifying volume flow. In modern magnet installations, eddy currents are largely eliminated by shielded gradients. The influence of such baseline offset is dependent on the velocity sensitivity, the higher the velocity sensitivity, the smaller the effect of the baseline offset. The phase error increases if the electrical conductivity of the sample or the switched gradient amplitudes are higher [109]. The phase error is also dependent on the shape of the velocity-encoding gradients. To reduce signal loss caused by complex flow (acceleration, jerk, etc.), the duration and amplitude of the gradient in the direction of flow must be reduced [85, 121, 124, 125].

Misregistration artifacts; spatial and velocity displacement

Misalignment between the direction of flow and the direction of motion-encoding G(t) causes error in flow measurement. Generally, a scout image is obtained first and used to position the slices perpendicular to the imaging plane. The true flow values can be calculated from the measured values, if the angle of misalignment is known.

The velocity displacement artifact is a phenomenon that arises when spins are moving during the time needed for spatial encoding [126, 127]. The second type of artifact arises from the acceleration of spins during spatial- and velocity encoding. Such artifacts can lead to errors in velocity measurements, especially in the presence of oblique and accelerating flows [128-130].

In the present study only the component of flow perpendicular to image plane was measured. The 3-D encoding is possible but would have compromised the temporal resolution of flow measurements. Also in the phantom, in the left ventricular outflow and in the mitral transannular flow study the velocity components in-plane are likely to be negligible.

A regular cardiac rhythm prevents ghosting. Misregistration can be minimized by ensuring that the motion-encoding corresponds the flow directions and by using ultrashort times for spatial encoding.

Higher-order velocity components

In the human body acceleration is often present in blood flow. This can be in the form of pulsatile flow or even in steady flow caused by bending or narrowing of the vessel. Higher order motion components due to complex flow patterns can give rise to significant additional $\Delta\phi$ errors in the velocity measurements, thus causing errors in the estimated velocity. Taylor expansion (Eq. 1) can be used to locally expand the location time function of pulsatile flow in position, velocity, acceleration, jerk, and higher-order motion derivatives.

An efficient way to reduce the sensitivity to higher-order motion is to reduce the duration of the motion-encoding gradient field [85, 131, 132]. The phase variance within a voxel increases with the percentage of echo acquired [85]. By acquiring partial echoes, intravoxel dephasing can be reduced significantly in complex and simple laminar flows.

Placement of ROI

Volume flow in a vessel can be quantified from a through-plane velocity map as the average velocity within an ROI multiplied by the cross-sectional area of the ROI. The changes in shape of the vessel cross section over the cardiac cycle requires the user to trace the luminal border of the vessel in each individual phase of the MR examination.

A pair of images is typically generated in PCVM measurements: a magnitude image and a phase difference image. The ROI is often drawn on a magnitude image in which the blood vessel appears bright. The vessel boundary can be characterized by a transition of image intensity from bright (within the vessel) to medium (within the vascular wall). Local intensity profiles at the transition from blood to vascular wall are subject to wide variability, due to volume averaging and flow and motion artifacts.

If the ROI size is smaller than the section of the vessel, the volume flow is underestimated. If the ROI is much larger than the lumen of the vessel, the flow-related $\Delta\phi$ will vanish within the noise from the stationary tissue, due to the limited SNR [133].

RF saturation

In RF saturation successive pulses partially the saturate the moving spins. Slower-moving spins experience more RF pulses than fast moving spins and are more saturated, which result in overestimation of the mean velocity of the blood flow. Both the PD and CD methods suffers from saturation effects related to through-plane motion [134]. These saturation effects can also be decreased by using T1-shortening contrast agents, long TRs, and/or k-space segmentation in the pulse sequence.

Velocity-encoding parameter (Venc)

PCVM requires selection of the velocity-encoding parameter (Venc). Venc is the the most rapid flow velocity that can be imaged without flow-related aliasing, i.e. it produces $\Delta\phi$ of π radians;

$$Venc = \pi /(\gamma \Delta M_1), \quad (13)$$

where ΔM_1 is the change in the first moment. The measured $\Delta\phi$ in degrees can be converted to velocity v by:

$$v = (\Delta\phi / 180)Venc \quad (14)$$

Thus the encoded velocity limits the measurable velocity range. The SNR in PCVM is proportional to v/Venc, where v is the velocity of flowing blood. Therefore, it is advantageous to reduce Venc as much as possible, but not smaller than the highest velocities in the flow. Phase wraparound occurs due to the fact that phase takes values between $-\pi$ and $+\pi$ radians. The velocity values outside the sensitivity range will wrap around, resulting in apparent reversal of direction.

The velocity-induced $\Delta\phi$ must significantly exceed the random variation of the phase [135]. If the Venc is too large, the SNR will be low. If the Venc value is too small, phase-aliasing will result. The predicted peak velocity should cover approximately two-thirds of the available phase interval to avoid aliasing of the velocity data while retaining adequate sensitivity [131].

7.2.2.1.2 Precision

The relationship between the phase image velocity-to-noise ratio VNR and the magnitude image SNR in PCVM measurements is given by the following expression

$$VNR = \frac{\pi \upsilon}{\sqrt{2} v_{enc}} SNR \quad (15)$$

where Venc is the velocity-encoding parameter and v the velocity [136].

It was shown in an in vivo aortic flow study that in addition to the usual scanning parameters such as TR, TE, and FA, the zero velocity (background) pixel value, size and shape of the vessel ROI, the maximum velocity encoded, and temporal resolution had a much greater effect on the flow measurements [135].

7.2.2.2 Sources of errors in segmented cine PCVM

Blurring

K-space segmentation leads to prolongation of the acquisition window for each phase within cardiac cycle. This causes blurring in the magnitude and phase images during motion of the vessel [137, 138]. The larger is the LPS; the worse is the

blurring. The blurring results in increasing difficulties in identifying the margins of the moving vessel.

Effects of ROI Size, FOV, Matrix, and Angle

As long as the ROI size was equal to the vessel size, the accuracy of flow measurements appeared to be independent of FOV, matrix size, and misangulation below 20^0 [120]. If the ROI size is increased segmented sequences tend to result in overestimation of flow more than conventional sequences. Underestimation of flow occurred when the ROI size was smaller than the vessel size. An overestimation of flow occurred when the ROI size was larger than the actual vessel size. This overestimation has been further enhanced by misangulation of the image plane relative to the flow direction [120].

7.2.3 Sequence-optimization methods

The PCVM method always suffers from the associated compromise between precision, total imaging time, and spatial and temporal resolution. The phase spread is most prominent at the tube edge and decreases toward the center. When stationary spins are present in the imaging voxels they lead to underestimation of the velocity of the moving spins [139]. Several methods were proposed for correction of partial volume errors [90, 140]. The spatial resolution chosen should be maximal, which aids in minimizing signal intensity loss and partial-volume effect [122]. It was shown that accurate flow measurements can be achieved for vessels occupying more than about 16 pixels [139]. When volume flow was measured in the present study the number of pixels was well above 16. If resolution is low, the ROI selected will be larger than the actual vessel area because the point spread function (PSF) causes a broadening of the vessel outline. Partial-volume effects can also occur in the slice direction if the imaging plane is not perpendicular to the vessel wall or when the vessel is curved. The present studies (I, II, IV) focused on the systolic peak. Systolic flow profiles are more plug-shaped, with relatively high velocities near the wall. This results in additional partial-volume error and inflow enhancement, which increases the error.

A relatively small FA was used to minimize the signal difference between flowing blood and the surrounding stationary tissue. This reduced the partial-volume effect by reducing the inflow enhancement, especially when PD subtraction was used. However, using too small an FA also means a lower SNR. In the present paper, the relative low SNR was due to the use of the body coil as an RF receiver during the in vivo studies. To maximize SNR in blood Ernst angle (θ_E) can be used. It determines the FA that maximizes the signal-per-unit time in a GRE sequence and is given by the equation

$$\theta_E = \cos^{-1}(e^{-TR/T1}), \qquad (16)$$

where T1 is the longitudinal relaxation time of the blood and TR the repetition time. The T1 of blood is dependent on the oxygen (O_2) concentration [141]. In the present study the oxygen concentration was high in the mitral transannular flow and left ventricular outflow tract, as well as in the aorta. Thus, the T1 of blood at 1.5 T was 1300 ms and at 1.0 T 1200 ms. In the present flow-sensitive studies, TR changes

from 25 to 43 ms, implying that the optimal FA in Eq. 10 varies from 12^o to 15^o. However, the θ_E calculation does not take into account the flow-related enhancement effects, which tends to result in underestimation of the optimum FA in the PCVM measurements, hence the FA of 30^o used in the present study to give high SNR.

In the present study the ROI was drawn manually. MR images suffer from a relatively low SNR and are degraded by flow and motion artifacts, which makes automated edge-detection methods difficult to work reliably. If the magnitude image was used to draw the ROI, adjustment of the ROI was often necessary when it was transferred over the phase image. The main reason for the shift is the difference between two phase images obtained at different time points whereas the magnitude image was chosen at one of these time points.

In the phantom measurements the ROI was chosen to be smaller than actual diameter of the tube to avoid large amounts of error introduced into the velocity measurement by the large random phase noise found on the tubing wall. This resulted in underestimation of the volume flow rate and overestimation of the mean velocity. However, obtaining absolute values for these parameters was not the focus here. Near-wall measurements also suffer from magnetic susceptibility artifacts.

In the left ventricular outflow tract study (II) the image plane was placed 0.5-1.0 cm below the level of the aortic annulus. Flow measurements are most accurate when the slice is placed between the aortic valve and the coronary ostia [22]. However, movement of the aortic valve perpendicular to the image slice in our experience can be as much as 1-2 cm during the R-R interval, which make positioning inaccurate. The problem of perpendicular movement could have been lessened somewhat by acquiring several image slices. The cyclical movement of the outflow area in the image plane in the mediolateral and anteroposterior direction was accounted for by defining the ROIs frame-by-frame.

The artifactual $\Delta\phi$ caused by local eddy currents, inhomogeneities in the main field, and concomitant G(t) errors was corrected by measuring the phase offset near the lumen. A circular ROI with an area of several centimeters squared was placed in the background, the ROI did not include the lumen itself. We assumed that the ROI area was stationary and assigned it a zero-velocity value. However the background may also contain random phase voxels that could have resulted in error. A constant phase background can be corrected, but a random phase background simply adds to the imprecision of measurement. The reference ROI for performing a baseline correction is especially important when low velocities are analyzed.

Physiological flow waveforms are not absolutely repetitive [142]. Cycle-to-cycle variations in human flow waveforms are generally observed. This variability leads to errors in mean and instantaneous flow rates in cardiac-gated techniques.

Velocity displacement artifacts are stronger for pulsatile flow than for steady flow. These artifacts can lead to errors in velocity measurements, particularly in the presence of obliqueness and acceleration [125]. In some studies (I, II, IV) velocities were measured with gated studies of pulsatile flow and special focus was on the systolic peak. As velocity displacement artifact led to incorrect velocities in the correct places, the spatial displacement artifact served to assign the correct velocities

in the incorrect places. Both displacement artifacts are most prominent near peak systole. During in vitro experiments artifacts caused by obliqueness were avoided by carefully placing the slice direction along the model z-axis. In vivo measurements were also acquired by selecting a straight vessel segment and positioning the scanning plane normal to the flow streamlines. This also minimized the partial-volume effects. The misalignment was, however, compensated for the increase in cross-sectional area. The consequences of misalignment are small in clinical MR velocity measurements.

In the present studies (II-IV) the flows formed complex patterns. Spin saturation and phase dispersion in complex transient recirculation zones are significant contributors of overall error. The SNR in the recirculation area is reduced as a result of spin saturation and phase dispersion. To reduce the effect of possible phase dispersion, fractional echo sampling (50%) was used. Thus TE was reduced to 5 ms. The velocity-induced phase dispersion resulted in underestimation of the flow rate. The partial echo technique should be used when measuring complex flows, whereas in conditions of steady flow partial echoes can induce additional phase errors.

To decrease the error caused by acceleration and deceleration, second-order moment of the gradient was not compensated to zero. This suggests that the PCVM measurements were overestimated during the period of acceleration and underestimated during the deceleration of the pulsatile flow. However, using the second-order flow compensation would have increased TR.

Eq. (15) shows that the noise in the phase images is independent of the phase itself and merely determined by the SNR of the magnitude image and Venc. This implies that the absolute precision of velocity measurement can be determined by adjusting the velocity sensitivity or manipulating the sequence parameters and RF coils that determine the level of SNR from the magnitude image. The Venc was set above the maximum velocity anticipated in the vessel (or tube) of interest to prevent aliasing, which results in false velocity values. Some errors can be corrected by postprocessing. In the present study the Venc was as close to the maximum velocity as possible to achieve minimum random error. Higher velocity sensitivity requires a larger velocity encoding gradient pulse and therefore a longer TE. Long TE result in phase errors in the complex flow patterns, and if the increase in TE is significant the SNR is decreased.

Although higher Venc values do not result in significant errors, they cause decrease in velocity resolution and thus may influence peak flow velocity measurements and reduce the ability to distinguish slow-flowing blood. The correct choice of the Venc value was important in the present study in which we attempted to find small changes in velocity profiles.

Since the data were sampled over several ECG cycles, changes in velocities from one k-space line to another resulted in different velocity-induced first-order signal phases. If the patient’s heart rate changes ECG triggering is hampered, leading to problems in obtaining true end-velocity maps.

Segmented cine PCVM

ECG gating successfully eliminates artifacts from cardiac motion, but the patient's breathing during acquisition still results in image blurring and ghosting. Segmented cine GRE was used to collect a full velocity map during breath-hold and to improve edge detection. Using segmented cine PCVM respiratory ghosting could be avoided, less blurring of vascular structures occured, and artifacts caused by arrhythmia were reduced. Several groups also reported using the k-space segmentation technique in animal and human coronary arteries [143-145].

In the present study the effect of LPS on quantitative accuracy of segmented PCVM for pulsatile and continuous flows in the phantom were determined. However, the use of a rigid tube did not mimic the compliant properties of veins, and thus the phantom study has its limitations when compared to flow measurements in vivo.

As the number of LPS increased the data acquisition window for each phase within the cardiac cycle was increased. Longer data acquisition window caused more blurring to the magnitude and phase images. Because of the vessel movement the blurring became worse during measurements in vivo. The blurring made it more difficult to identify the margins of the vessel than in conventional PCVM, which could have affected the accuracy of the flow measurements.

In the present study a temporal shift in the flow curves was observed, therefore an adjustment had to be performed so that the time corresponding to any time phase would have been the time of acquisition of the central k-space line of the segment. For all segmented sequences the most important velocity information is contained in the most central k-space line of the segment.

The segmented PCVM sequences resulted in greater overestimation of the average flow more than conventional PCVM when the ROI size or FOV was increased. If the ROI is smaller than the lumen, the mean velocity will be underestimated.

Only minor changes were observed in measured mean velocity when LPS was changed, even with relative broad data acquisition windows of 63 – 231 ms. The average measured remained close to the true values.

When the number of LPS was increased, the number of cardiac phases was reduced but fewer heartbeats were required to complete the acquisition. Thus the length of breath-hold period can be adjusted by changing the number of LPS. When both velocity-sensitized and velocity-compensated gradient pulses are interleaved the number of cardiac cycles are equal to the phase-encoding steps divided by two the number of LPS and the scanning time is equal to the number of cardiac cycles times the R-R interval. Segmented cine PCVM result in overestimation of the temporal mean velocity of pulsatile flow, especially with large numbers of LPS, possible due to signal and phase modulation of the pulsatile flow or inadequate sampling rate [146].

Various optimized phase-ordering schemes have been introduced. The sequential phase-encode scheme acquires the central portion of the k-space and leads to significant blurring and ghosting artifacts that become worse when the LPS is increased. We used the simple segmented scheme described in part V. In this

method the central phase-encoding step occurs at the same time point in the cardiac cycle. Thus blurring and ghosting do not increase when the LPS in increased. Further improvement is obtained in a symmetrical centrally ordered fashion, which gives even better temporal localization of the velocity measurement in pulsatile flow [147] and also minimizes motion blurring and the mean $\Delta\phi$ error due to signal modulation of the pulsatile flow. Eddy currents resulted in some artifacts. Acquiring positive and negative regions of k-space separately followed by each other could have minimized this.

Large LPS values (LPS > 7) resulted in overestimation of the temporal mean velocity of pulsatile flow. We concluded that LPS values > 5 are not clinically relevant. However, new magnet devices with better gradients and shimming recently showed that also LPS 7 or even LPS 9 are clinically usable [106]. More powerful gradient systems and so-called view sharing can also improve the temporal resolution in segmented measurements. With the new MRI scanners complete cine acquisition of 17–25 cardiac phases in 20 s for a rate of 60 cycles/min can be acquired using 7 k-space LPS. The data acquisition window per phase become wider when using LPS of 9 or more. This can cause problems in adequately resolving rapidly changing flow waveforms, e.g. in the aorta during systole. Low-pass filtering of velocity information was expected. This occured even though the central Fourier lines were obtained at approximately same TD.

7.2.3.1 Aortic distensibility

Area based method

The cine MRI method of assessing aortic distensibility by evaluating the diastolic and systolic aortic luminal area was developed in previous studies [26, 33, 34, 148, 149]. The method is based on finding the smallest and largest circumferences of the ascending and descending thoracic aorta, using cine MR images. The cine sequence must provide dynamic images with good blood-signal enhancement at high temporal resolution (short TR).

In the present study a cine FISP sequence with TR of 50 ms and TE of 12 ms was used to examine the pulsatile changes in the cross sectional luminal areas. Sharp definition of the lumen edge is necessary for be able to delineation of the luminal area. Therefore, flow compensation was used in the slice-selection direction, which reduced blurring and added contrast to the lumen. The circumferences were traced manually with a mouse-driven cursor in an off-line image analysis system. The tracing was repeated to ensure the consistency of the results.

Assessment of the reproducibility of the cine MRI measurements was also done. Eight volunteers were examined twice one week apart. The data on luminal area change, areal strain, and aortic E_ρ fluctuated with mean reproducibility between 20% and 25%, which is less than ideal. One problem was spatial resolution; the pixel size was 2.7x1.4 mm^2 and the slice thickness 7 mm, which causes large partial-volume effects. To minimize the partial-volume effect and to obtain correct areal sizes it is important to place the imaging plane exactly perpendicular to the ascending and descending aorta. Another explanation for the less than ideal repeatability observed is that both errors in measuring the diastolic and systolic areas may contribute to the

variation in pulsatile area change. The true change in the aortic luminal area is small when compared with the random error in the areal measurements. Movement of the aorta, particularly the ascending aorta, resulted in slight shifting of the slice in different phases of the cardiac cycle. Using several imaging planes and averaging the data could have reduced the influence of the measurement error. Furthermore, repeating the image analysis several times and averaging could have reduced the measurement error. TE was chosen as small as possible with the MR system used.

Aortic stiffness estimation using flow-wave velocity

Another method for assessment of aortic stiffness is the use of the FWV in the thoracic aorta as an index of aortic rigidity. The mean velocity-time curves were reconstructed separately for the cross-sections of the ascending and descending thoracic aorta. The sequence was based on the conventional FLASH sequence and uses interleaved acquisition of flow-compensated and of flow-sensitive GRE signals.

The aortic FWV was reduced with antihypertensive treatment, but the changes were not statistically significant. The FWV is related in principle in a linear manner to the square root of Peterson's volume E_p. Some differences resulted from by the fact that the aortic E_p data represent purely local aortic function, whereas the FWVs were calculated over a much longer aortic segment, from the ascending part over the arch to the descending segment of the ascending aorta. The major source of error in PWV measurements in the present study lies in extrapolation of the upstroke of the curve to the baseline. This could have been improved by increasing the time resolution with repeated measurement and trigger delays, as was done in the phantom study (I). Deriving compliance from PWV measurements can be difficult because it requires knowledge of the cross-sectional area. To determine accurate area a second scan with a specially optimized acquisition sequence is needed.

7.2.3.2 Volumetric measurements

Our studies showed that cine GRE imaging can provide an accurate method for measurement of cardiac ventricular volumes in vivo and vitro. However, the disadvantages of the method are its relative long acquisition times and sensitivity to motion. These limitations may be overcome using segmented k-space cine sequences [79, 117, 150].

High contrast between the myocardium and intraventricular cavity is crucial for accurate assessment of ventricular volumes. The FISP and FLASH cine imaging used can provide multiple frames in a single slice with good contrast between the myocardium and blood. FISP produces clearer images with greater contrast at the endocardial border. However, FISP is more sensitive to artifacts from field inhomogeneities, susceptibility effects, and artifacts related to eddy current induction. These characteristics show that cardiac volumes may differ significantly between FISP and FLASH sequences [151]. Some of the FISP-FLASH differences are likely to be flow-related at the complicated blood-myocardium interfaces. In the atrial studies the problem of nonexisting borders occurs during diastole when the atrioventricular valves are open.

7.3 Future prospects for cine imaging

Cine PCVM

Although in the present study the ROIs were drawn manually various semiautomatic and automatic vessel edge-detection algorithms were proposed [152]. These methods should improve reproducibility and accuracy in postprocessing analysis. A different method for compensating phase aliasing with post-prosessing has also been proposed. By allowing aliasing and using aliased velocity correction, VNR can be improved considerably [119, 153, 154]. In the present study no phase-unwrapping method was available.

Further improvement in temporal and spatial resolution in PC cine MRI can be achieved with view-sharing techniques [155]. The velocity induced $\Delta\phi$ in PC are mainly encoded in the central region of the k-space, which makes view sharing suitable for PCVM. View sharing could also be used to maintain the number of reconstructed image frames as the LPS was increased. Using higher-performance gradients it is also possible to increase the number of phase-encoding lines per cardiac cycle resulting in more rapid imaging or better image resolution per time unit.

With the sensitivity encoding (SENSE) and the simultaneous acquisition of spatial harmonics (SMASH) parallel acquisition techniques it is possible to reduce cine imaging scanning times and obtain higher resolution or better volume coverage, although there is usually some lose in SNR [156, 157]. It is possible to achieve accurate flow measurements even at high reduction factors with PCVM, using SENSE [158].

Nonvelocity-sensitive cine imaging

Other studies have also advocated the use of intravascular contrast agents in conjunction with cine MRI [159]. Cine TrueFISP for cardiac cine MRI, employing high signal at short TR, may represent an alternative. The contrast of TrueFISP is depend mainly on the tissue T1:T2 ratio and not on through-plane flow. Due to the high inherent contrast between the myocardium and ventricular cavity and motion insensitivity, the automated segmentation process in the TrueFISP sequence apparently provides more reliable results in comparison to standard FLASH images [160]. TrueFISP obviates the need for intravascular contrast agents. The contrast between blood and myocardium can still be enhanced using dual-FA TrueFisp [161]. This improves the accuracy of the automatic and semiautomatic segmentation process.

Fast-gradient and intravascular contrast agents have recently allowed for 3-D cardiac cine MRI using respiratory compensation [162]. Gated 3-D volume acquisition in breath-hold was recently introduced [163]. Gated 3-D TrueFISP allows the complete heart to be acquired in its systolic phase within about 20 heartbeats with a resolution of 2*2*3 mm [164]. The 3-D cine datasets have typically temporal resolutions on the order of 70 ms [159].

Cardiac imaging at high field strength (3T) results in higher SNRs compared with 1.5 T as shown by an increase of 20 - 85% and ventricular blood-myocardium CNR

greater than 30% [165]. The increase in SNR can be exploited by reducing the voxel size or acquisition times.

8 CONCLUSION

The results of this study suggest that conventional and segmented k-space MRI PCVM can be used for accurate flow quantification under conditions of steady and pulsatile flow. In the present study we examined this in both nonpulsatile and pulsatile flow using a stationary phantom (I). The segmented k-space acquisition makes it possible to image reliably multiframe cine flow images (< 7 LPS) in timescale of a single breath-hold.

Conventional PCVM was applied to the complex intracardiac flow. In the present studies for the first time the reconstructions of spatially complete cross sectional flow velocity maps in the left ventricular outflow tract and mitral annulus in healthy human volunteers were accomplished. The previously assumed idea in the ultrasound flow measurements of spatial homogeneity of flow in these areas was questioned. Despite the possible measurement error sources, these studies have revealed a significant spatial inhomogeneity in both regions (In the left ventricular outflow tract; the inhomogeneity of the mean flow rate was 19.2% $\pm$ 3.5%, in the mitral annulus flow; the inhomogeneity averaged 33.5 $\pm$ 13.8% for early velocity peak, 41.1 $\pm$ 16.1% for the late diastolic velocity peak, and 70.0 $\pm$ 33.9% for the mean diastolic flow rate).

Measuring pulsatile changes of the cross-sectional luminal areas and FWV, cine MRI can be employed to evaluate aortic distensibility with the limitation of not so ideal repeatability.

Nonvelocity-sensitive GRE cine MRI can be successfully applied in cardiac atrial volumetry and function estimations. The left and right atrial casts correlated closely ($r = 0.99$, $p < 0.001$) with the true volumes, even though small underestimation was observed. The method is well applicable also to right ventricular volume measurements in vitro by proper selection of slice direction (the mean absolute difference from the true right ventricular volume was 0.2 $\pm$ 1.6 ml).

ACKNOWLEDGEMENTS

The present study was carried out in the MRI Unit at the Department of Radiology, Helsinki University Central Hospital, during the years 1994-1998. I would like to express my gratitude to Carl-Gustaf Standertskjöld-Nordenstam, Professor (Emer.) of Diagnostic Radiology and Juhani Keinonen, Professor, Head of the Department of Physical Sciences, for their encouraging support and for placing the facilities of the Departments at my disposal. Professor Standertskjöld-Nordenstam and my predecessor Leena Hamberg, Ph.D., invited me initially to work in the Department and to become a hospital physicist.

I thank my supervisors, Docent Sauli Savolainen, Ph.D., and Docent Pauli Hekali, M.D., for their guidance. They deserve thanks for having faith in my career possibilities. Sauli Savolainen suggested to me the idea to write the thesis in this form. Pauli Hekali originally introduced me to the idea of becoming part of cardiovascular MRI research team. This fruitful cooperation has continued ever since the first clinical high-field magnet scanner in Finland was installed in Meilahti Hospital. Pauli's support and guidance have enabled me to carry through this work.

To my official reviewers, Professor Raimo Sepponen and Docent Pekka Niemi, I wish to express my profound gratitude for their constructive comments and advice that have markedly improved this thesis.

I thank all the co-authors of the original articles. I am very grateful to Docent Markku Kupari, M.D.. Most of the ideas on how to apply cine MRI in clinical studies originated from him. Without the help of Vesa Järvinen, M.D, Aslak Savolainen, M.D., and Tommi Jauhianen, M.D., this thesis would have been impossible to carry out. Many of the practical work and MRI measurements were done together with Vesa Järvinen, who deserves my special thanks.

Many practical in vivo sessions were performed with Riku Kivisaari, M.D.. His diligence and initiative have been invaluable in this study. I also want to thank Docent Anna-Maija Häkkinen, who always found time for her generous help throughout this project.

I want to thank Tapio Paananen, M.D., for many critical discussions concerning the methodology of the study. He has also increased my knowledge in the field of cardiac radiology and given me technical help. My special thanks go to Professor Leena Kivisaari who encouraged me to continue this work. My colleague and friend Tapani Korppi-Tommola, Ph.Lic., has supported and encouraged me and given his time for revising the language.

Finally, I want to express my warmest thanks to my beautiful wife Outi, who has given her firm support to my efforts, and to my children Mira, Kristian, Meri, Kiia, and Kaius for their patience and giving me the time to fulfil this work.

This study was financially supported by the Radiological Society of Finland, the state subsidy for University Hospitals, and Instrumentarium Science Foundation, which I gratefully acknowledge.

REFERENCES

1. Wyman, R., R. Safian, V. Portway, J. Skillmann, R. McKay, and D. Baim, *Current complications of diagnostic and therapeutic cardiac catheterization.* Journal of the American College of Cardiology, 1988. 12(6): p. 1400-1406.

2. Vallejo, E., D. Dione, W. Bruni, R. Constable, P. Borek, J. Soares, J. Car, S. Condos, F. Wackers, and A. Sinusas, *Reproducibility and accuracy of gated SPECT for determination of left ventricular volumes and ejection fraction: experimental validation using MRI.* Journal of Nuclear Medicine, 2000. 41(5): p. 874-882.

3. Singer, J., *Blood flow rates by NMR measurements.* Science, 1959. 130: p. 1652-1653.

4. Jones, D. and T. Child, *NMR in flowing system.* Advanced Magnetic Resonance, 1976. 8: p. 123-148.

5. Zhernovoi, A. and G. Latyshev, *Nuclear magnetic resonance in a flowing liquid*, ed. T.T. Translated from Russian by Turton CN. 1965, New York: Consultants Bureau.

6. Singer, J. and L. Crooks, *Nuclear magnetic resonance blood flow measurements in the human brain.* Science, 1983. 221: p. 654-656.

7. Mueller, E., M. Deimling, and E. Reinhardt, *Quantification of pulsatile flow in MRI by an analysis of T_2 changes in ECG-gated multiecho experiments.* Magnetic Resonance in Medicine, 1986. 3: p. 331-335.

8. Wehrli, F., A. Shimakawa, G. Gullberg, and J. MacFall, *Time-of-flight MR-flow imaging: Selective saturation recovery with gradient refocusing.* Radiology, 1986. 160: p. 781-785.

9. Moran, P., *A flow velocity zeugmatographic interlace for NMR imaging in humans.* Magnetic Resonance Imaging, 1982. 1: p. 197-203.

10. Moran, P., R. Moran, and N. Karstaedt, *Verification and evaluation of internal flow and motion.* Radiology, 1985. 154: p. 537-545.

11. van Dijk, J., *Direct cardiac NMR imaging of heart wall and blood flow velocity.* Journal of Computer Assisted Tomography, 1984. 8: p. 429-436.

12. Bryant, D., J. Payne, D. Firmin, and D. Longmore, *Measurement of flow with NMR using gradient pulse and phase difference techniques.* Journal of Computer Assisted Tomography, 1984. 8: p. 588-593.

13. Bradley, W. and V. Waluch, *Blood flow: magnetic resonance imaging.* Radiology, 1985. 154: p. 443 - 450.

14. Nayler, G., D. Firmin, and D. Longmore, *Blood flow imaging by cine magnetic resonance.* Journal of Computer Assisted Tomography, 1986. 10(5): p. 715-722.

15. Nishimura, R., C. Rihal, A. Tajik, and D. Holmes, *Accurate measurement of transmitral gradient in patients with mitral stenosis: a simultaneous catheterization and Doppler echocardiographic study.* Journal of the American College of Cardiology, 1994. 22(1): p. 152-158.

16. Kunz, K., J. Polak, A. Whittemore, J. Skillmann, and K. Kent, *Duplex ultrasound criteria for the identification of carotid stenosis should be labarotory specific.* Stroke, 1997. 28(3): p. 597-602.

17. Meyer, J., R. Khalil, N. Obuchowski, and L. Baus, *Common carotid artery: variability of Doppler US velocity measurements.* Radiology, 1997. 204(2): p. 339-341.

18. Mikkonen, R., J. Kreula, and P. Virkkunen, *Reliability of Doppler ultrasound in follow-up studies.* Acta Radiologica, 1998. 39(2): p. 193-199.

19. Evans, A., R. Blinder, R. Herfkens, C. Spritzer, D. Kuethe, E. Fram, and L. Hedlund, *Effects of turbulence on signal intensity in gradient echo images.* Investigative Radiology, 1988. 23(7): p. 512-518.

20. Sechtem, U., P. Pflugfelder, R. White, R. Gould, W. Holt, M. Lipton, and C. Higgins, *Cine MR imaging; potential for the evaluation of cardiovascular function.* American Journal of Roentgenology, 1987. 148(2): p. 239-246.

21. Galea, D., M. Lauzon, and M. Drangova, *Peak velocity determination using fast Fourier velocity encoding with minimal spatial encoding.* Medical Physics, 2002. 29(8): p. 1719-1728.

22. Chatzimavroudis, G., P. Walker, J. Oshinski, R. Franch, R. Pettigrew, and A. Yoganathan, *Slice location dependence of aortic regurgitation measurements with MR phase velocity mapping.* Magnetic Resonance in Medicine, 1997. 37(4): p. 545-551.

23. Ledesma-Carbayo, M., J. Kybic, M. Desco, A. Santos, and M. Unser, *Cardiac motion analysis from ultrasound sequences using non-rigid registration*, in *Lecture Notes in Computer Science*, W.N.a.M. Viergever, Editor. 2001, Springer-Verlag: Heidelberg. p. 889-896.

24. Kon, M., F. Wiesmann, N. Moat, and D. Pennell. *Selection of imaging level for magnetic resonance phase velocity mapping in the quantification of aortic regurgitation - a comparison with a volumetric method*. in *Proceeding of the 6th Annual Meeting of International Society for Magnetic Resonance in Medicine*. 1998. Sydney, Australia.

25. Mohiaddin, R. and D. Longmore, *Functional aspects of cardiovascular nuclear magnetic resonance imaging: techniques and applications.* Circulation, 1993. 88(1): p. 364-281.

26. Kupari, M., P. Keto, P. Hekali, V.-P. Poutanen, A. Savolainen, and C.-G. Standertskjöld-Nordenstam, *Cine magnetic resonance imaging in assessment of aortic distensibility.*, in *Functional abnormalities of the aorta*, T.P. Boudoulas H, Wooley CF, Editor. 1996, Futura Publishing Co., Inc.: Armonk, NY.

27. Urschel, C., J. Covell, E. Sonnenblick, J. Ross, and E. Braunwald, *Effects of decreased aortic compliance on performance of the left ventricle.* American Journal of Physiology, 1968. 214(2): p. 298-304.

28. Sunagawa, K., W. Maugham, and K. Sagawa, *Stroke volume effect of changing arterial input impedance over selected frequency ranges.* American Journal of Physiology, 1985. 248(4 Pt 2): p. 477-484.

29. Bogren, H., R. Mohiaddin, R. Klipstein, D. Firmin, R. Underwood, S. Rees, and D. Longmore, *The function of the aorta in ischemic heart disease: a magnetic resonance and angiographic study of aortic compliance and blood flow patterns.* American Heart Journal, 1989. 118(2): p. 234-247.

30. Liu, Z., C. Ting, S. Zhu, and F. Yin, *Aortic compliance in human hypertension.* Hypertension, 1989. 14(2): p. 129-136.

31. Mohiaddin, R., S. Underwood, H. Bogren, D. Firmin, R. Klipstein, R. Rees, and D. Longmore, *Regional aortic compliance studied by magnetic resonance imaging: the effects of age, training and coronary artery disease.* British Heart Journal, 1989. 62(2): p. 90-96.

32. Hickler, R., *Aortic and large artery stiffness: current methology and clinical correlations.* Clinical Cardiology, 1990. 13(5): p. 317-322.

33. Savolainen, A., P. Keto, P. Hekali, L. Nisula, I. Kaitila, M. Viitasalo, V.-P. Poutanen, C.-G. Standertskjöld-Nordenstam, and M. Kupari, *Aortic distensibility in children with the marfan syndrome.* The American Journal of Cardiology, 1992. 70(6): p. 691-693.

34. Savolainen, A., P. Keto, P. Hekali, L. Nisula, I. Kaitila, M. Viitasalo, V.-P. Poutanen, C.-G. Standertskjöld-Nordenstam, and M. Kupari, *Regional aortic compliance in Marfan's syndrome.* European Heart Journal, 1991. 12.

35. Hirai, T., S. Sasayama, T. Kawasaki, and S. Yagi, *Stiffness of systemic arteries in patients with myoacardial infarction. A nonoinvasive method to predict severity of coronary artherosclerosis.* Circulation, 1989. 80(1): p. 78-86.

36. Peterson, L., R. Jensen, and J. Parnell, *Mechanical properties of arteries in vivo.* Circulation Research, 1960. 8: p. 622-639.

37. Bock, M., L. Schad, E. Muller, and W. Lorenz, *Pulsewave velocity measurement using new real-time MR-method.* Magnetic Resonance Imaging, 1995. 13(1): p. 21-29.

38. Vulliemoz, S., N. Stergiopulos, and R. Meuli, *Estimation of local aortic elastic properties with MRI.* Magnetic Resonance in Medicine, 2002. 47(4): p. 649-654.

39. Mohiaddin, R., D. Firmin, and D. Longmore, *Age-related changes of human aortic flow wave velocity measured noninvasively by magnetic resonance imaging.* Journal of Applied Physiology, 1993. 74(1): p. 492-497.

40. Hardy, C., B. Bolster, E. McVeigh, W. Adams, and E. Zerhouni, *A one-dimensional velocity technique for NMR measurement of aortic distensibility.* Magnetic Resonance in Medicine, 1994. 31(5): p. 513-520.

41. Macgowan, C. and M. Wood. *One-dimensional particle tracking of fluid motion using tagging*. in *Proceeding of the 8th Annual Meeting of International Society for Magnetic Resonance in Medicine*. 2000. Denver, Colorado.

42. Rehr, R., C. Malloy, N. Filipchuk, and R. Peshock, *Left ventricular volumes measured by MR imaging.* Radiology, 1985. 156(3): p. 717-719.

43. Keller, A., R. Peshock, C. Malloy, L. Buja, R. Nunnally, R. Parkey, and J. Willerson, *In vivo measurement of myocardial mass using nuclear magnetic resonance imaging.* Journal of the American College of Cardiology, 1986. 8(1): p. 113-117.

44. Florentine, M., C. Grosskreutz, W. Chang, J. Hartnett, V. Dunn, J. Ehrhardt, S. Fleagle, S. Collins, M. Marcus, and D. Skorton, *Measurement of left ventricular mass in vivo using gated nuclear magnetic resonance imaging.* Journal of the American College of Cardiology., 1986. 8(1): p. 107-112.

45. Caputo, G., D. Tscholakoff, U. Sechtem, and C. Higgins, *Measurement of canine left ventricular mass by using MR imaging.* American Journal of Roentgenology, 1987. 148(1): p. 33-38.

46. Shapiro, E., W. Rogers, R. Beyar, R. Soulen, E. Zerhouni, J. Lima , and J. Weiss, *Determination of left ventricular mass by MRI in hearts deformed by acute infarction.* Circulation, 1989. 79(3): p. 706-711.

47. Bottini, P., A. Carr, L. Prisant, F. Flickinger, J. Allison, and J. Gottdiener, *Magnetic resonance imaging compared to echocardiography to assess left ventricular mass in the hypertensive patient.* American Journal of Hypertension, 1995. 8(3): p. 221-223.

48. Semelka, R., E. Tomei, S. Wagner, J. Mayo, G. Caputo, M. O'Sullivan, W. Parmley, K. Chatterjee, C. Wolfe, and C. Higgins, *Interstudy reproducibility of dimensional and functional measurements between cine magnetic resonance imaging studies in the morphologically abnormal left ventricle.* American Heart Journal, 1990. 119: p. 1367-1373.

49. Semelka, R., E. Tomei, S. Wagner, J. Mayo, C. Kondo, J. Suzuki, G. Caputo, and C. Higgins, *Normal left ventricular dimensions and function: interstudy reproducibility of measurements with cine MR imaging.* Radiology, 1990. 174(3 Pt 1): p. 763-768.

50. Pattynama, P., H. Lamb, E. van der Velde, E. van der Wall, and A. de Roos, *Left ventricular measurements with cine and spin-echo MR imaging: a study of*

reproducibility with variance component analysis. Radiology, 1993. 187(1): p. 261-268.

51. Katz, J., J. Whang, K. Boxt, and R. Barst, *Estimation of right ventricular mass in normal subjects and in patients with primary pulmonary hypertension by nuclear magnetic resonance imaging.* Journal of the American College of Cardiology, 1993. 21(6): p. 1475-1481.

52. Poutanen, T., A. Ikonen, P. Vainio, E. Jokinenl, and T. Tikanoja, *Left atrial volume assessed by transthoracic three dimensional echocardiography and magnetic resonance imaging: dynamic changes during the heart cycle in children.* Heart (British Cardiac Society), 2000. 83(5): p. 537-542.

53. Järvinen, V., M. Kupari, V.-P. Poutanen, and P. Hekali, *A simplified method for the determination of left atrial size and function using cine magnetic resonance imaging.* Magnetic Resonance Imaging, 1996. 14(3): p. 215-226.

54. Sandler, H. and H. Dodge, *The use of single plane angiocardiograms for the calculation of left ventricular volume in man.* American Heart Journal, 1968. 75: p. 325-334.

55. Dodge, H., H. Sandler, D. Ballew, and J. Lord, *The use of biplane angiocardiography for the measurement of left ventricular volume in man.* American Heart Journal, 1960. 60: p. 762-776.

56. Beier, J., T. Joerke, S. Lempert, E. Wellnhofer, H. Oswald, and E. Fleck, *A comparison of 7 different volumetry methods of left and right ventricle using post-mortem phantoms.* Instute of Electrical and Electronics Engineers, 1993: p. 33-36.

57. Järvinen, V., M. Kupari, V.-P. Poutanen, and P. Hekali, *Right and left atrial phasic volumetric function in mildly symptomatic dilated and hypertrophic cardiomyopathy: cine MR imaging assessment.* Radiology, 1996. 198(2): p. 487-495.

58. Järvinen, V., M. Kupari, P. Hekali, and V.-P. Poutanen, *Assessment of left atrial volumes and phasic function using cine magnetic resonance imaging in normal subjects.* The American Journal of Cardiology, 1994. 73(15): p. 1135-1138.

59. Reichek, N., *MRI myocardial tagging.* Journal of Magnetic Resonance Imaging, 1999. 10(5): p. 609-616.

60. Clark, N., N. Reichek, P. Bergey, E. Hoffman, D. Brownson, L. Palmon, and L. Axel, *Circumferential myocardial shortening in the normal human left ventricle. Assessment by magnetic resonance imaging using spatial modulation of magnetization.* Circulation, 1991. 84(1): p. 67-74.

61. Amoore, J. and J. Ridgway, *A system for cardiac and respiratory gating of a magnetic resonance imager.* Clinical Physics and Physiological Measurements, 1989. 10: p. 283 - 286.

62. Utz, J., R. Herfgens, J. Heinsimer, T. Bashore, R. Califf, G. Glover, N. Pelc, and A. Shimakawa, *Cine MR determination of left ventricular ejection fraction.* American Journal of Radiology, 1987. 148(5): p. 839-843.

63. Fletcher, B., M. Jacobstein, A. Nelson, T. Riemenschneider, and R. Alfidi, *Gated magnetic resonance imaging of congenital cardiac malformations.* Radiology, 1984. 150(1): p. 137-140.

64. Herfkens, R., *NMR assessment of valvular disease.* Radiology Medica, 1990. 80(1-2): p. 111-117.

65. Reeder, S., E. Atalar, A. Faranesh, and E. McVeigh, *Multi-echo segmented k-space imaging: an optimized hybrid sequence for ultrafast cardiac imaging.* Magnetic Resonance in Medicine, 1999. 41(2): p. 375–385.

66. Ding, S., S. Wolff, and F. Epstein, *Improved coverage in dynamic contrast-enhanced cardiac MRI using interleaved gradient-echo EPI.* Magnetic Resonance in Medicine, 1998. 39(4): p. 514-519.

67. Stuber, M., S. Fischer, M. Scheidegger, and P. Boesiger, *Toward high-resolution myocardial tagging.* Magnetic Resonance in Medicine, 1999. 41(3): p. 639–643.

68. Wielopolski, P., W. Manning, and R. Edelman, *Single breath-hold volumetric imaging of the heart using magnetization-prepared 3-dimensional segmented echo planar imaging.* Journal of Magnetic Resonance Imaging, 1995. 5(4): p. 403–409.

69. Slavin, G., S. Riederer, and R. Ehman, *Two-dimensional multishot echo-planar coronary MR angiography.* Magnetic Resonance in Medicine, 1998. 40(6): p. 883-889.

70. Higgins, C. and H. Sakuma, *Heart disease: functional evaluation with MR imaging.* Radiology, 1996. 199(2): p. 307-315.

71. De Roos, A., H. Kundel, P. Joseph, J. Doornbos, and H. Kressel, *Variability of myocardial signal on magnetic resonance images.* Investigative Radiology, 1990. 25(9): p. 1024-1028.

72. Lenz, G., E. Haacke, and R. White, *Retrospective cardiac gating: a review of technical aspects and future directions.* Magnetic Resonance Imaging, 1989. 7(5): p. 445-455.

73. Bohning, D., S. Carter, S. Liu, and G. Pohost, *PC-based system for retrospective cardiac and respiratory gating of NMR data.* Magnetic Resonance in Medicine, 1990. 16(2): p. 303-316.

74. Haase, A., J. Frahm, D. Mathaei, W. Haenicke, and K.-D. Merboldt, *FLASH imaging: rapid NMR imaging using low flip angles.* Journal of Magnetic Resonance, 1986. 67: p. 256-266.

75. Oppelt, A., R. Graumann, H. Barfuss, Fisher, W. Hartl, and W. Schajor, *FISP, a new fast MRI sequence.* Electromedica, 1986. 54: p. 15-18.

76. Scheffler, K. and J. Hennig, *Is TrueFISP a gradient-echo or spin-echo sequence?* Magnetic Resonance in Medicine, 2003. 49(2): p. 395 - 397.

77. Heid, O. *TrueFisp Cardiac Fluoroscopy*. in *Proceeding of the 5th Annual Meeting of International Society for Magnetic Resonance in Medicine*. 1997. Vancouver, Canada.

78. Matthaei, D., A. Haase, K. Merboldt, W. Hänicke, and M. Deimling, *ECG-triggered arterial FLASH-MR flow measurements using an external standard.* Magnetic Resonance Imaging, 1987. 5(5): p. 325-330.

79. Atkinson, D. and R. Edelman, *Cineangiography of the heart in a single breath hold with a segmented turboFLASH sequence.* Radiology, 1991. 178(2): p. 357-360.

80. NessAiver, M. *Relation between k-space trajectory and artifacts in breath held, gated segmented k-space imaging*. in *Proceeding of the 9th Annual Meeting of International Society for Magnetic Resonance in Medicine*. 2001. Glasgow, Scotland.

81. Bundy, J., O. Simonetti, G. Laub, and J. Finn. *Segmented TrueFISP cine imaging of the heart*. in *Proceeding of the 7th Annual Meeting of International Society for Magnetic Resonance in Medicine*. 1999. Philadelphia, Pennsylvania.

82. Haase, A., D. Matthaei, E. Bartkowski, E. Duhmke, and L. D, *Inversion recovery snapshot FLASH MR imaging.* Journal of Computer Assisted Tomography, 1989. 13(6): p. 1036-1040.

83. Matthaei, D., A. Haase, D. Henrich, and E. Duhmke, *Cardiac and vascular imaging with an MR snapshot technique.* Radiology, 1990. 177(2): p. 527-532.

84. Barkhousen, J., G. Laub, M. Goyen, J. Debatin, S. Ruehm, and M. Ladd. *Assessment of ventricular function in a single breath-hold using TrueFISP cine imaging*. in *Proceeding of the 9th Annual Meeting of International Society for Magnetic Resonance in Medicine*. 2001. Glasgow, Scotland.

85. Gatenby, J., T. McCauley, and J. Gore, *Mechanisms of signal loss in magnetic resonance imaging of stenoses.* Medical Physics, 1993. 20(4): p. 1049-1057.

86. Urchuk, S. and D. Plewes, *Mechanisms of flow-induced signal loss in MR angiography.* Journal of Magnetic Resonance Imaging, 1992. 2(4): p. 453-462.

87. Ståhlberg, F., L. Söndergaard, C. Thomsen, and O. Henriksen, *Quantification of complex flow using MR phase imaging--a study of parameters influencing the phase/velocity relation.* Magnetic Resonance Imaging, 1992. 10(1): p. 13-23.

88. Spritzer, C., N. Pelc, J. Lee, A. Evans, H. Sostman, and S. Riederer, *Rapid MR imaging of blood flow with a phase-sensitive, limited-flip-angle, gradient recalled pulse sequence: preliminary experience.* Radiology, 1990. 176(1): p. 255-262.

89. Firmin, D., L. Nayler, P. Kilner, and D. Longmore, *The application of phase shifts in NMR for flow measurement.* Magnetic Resonance in Medicine, 1990. 14(2): p. 230-241.

90. Polzin, J., M. Alley, F. Korosec, T. Grist, Y. Wang, and C. Mistretta, *A complex-difference phase-contrast technique for measument of volume flow rates.* Journal of Magnetic Resonance Imaging, 1995. 5(2): p. 129-137.

91. Firmin, D., L. Nayler, R. Klipstein, S. Underwood, and D. Longmore, *In vivo validation of MR velocity mapping.* Journal of Computer Assisted Tomography, 1987. 11(5): p. 751-756.

92. Meier, D., S. Maier, and P. Boesinger, *Quantitative flow measurements on phantoms and on blood vessels with MR.* Magnetic Resonance in Medicine, 1988. 8(1): p. 25-34.

93. Hartiala, J., G. Mostbeck, E. Foster, N. Fujita, A. Dulce, F. Chazouilleres, and C. Higgins, *Velocity-encoded cine MR in the evaluation of left ventricular diastolic function: measurement of mitral valve and pulmonary vein flow velocities and flow volume across the mitral valve.* American Heart Journal, 1993. 125(4): p. 1054-1066.

94. Zananiri, F., P. Jackson, P. Goddard, E. Davies, and P. Wells, *An evaluation of the accuracy of flow measurements using magnetic resonance imaging.* Journal of Medical Engineering & Technology, 1991. 15(4-5): p. 170-176.

95. Evans, A., F. Iwai, T. Grist, H. Sostman, L. Hedlund, C. Spritzer, R. Negro-Vilar, C. Beam, and N. Pelc, *Magnetic resonance imaging of blood flow with phase subraction tecnique. In vitro and in vivo validation.* Investigative Radiology, 1993. 28(2): p. 109-115.

96. Frayne, R., D. Steinman, C. Ethier, and B. Rutt, *Accuracy of MR phase contrast velocity measurements for unsteady flow.* Journal of Magnetic Resonance Imaging, 1995. 5(5): p. 428-431.

97. Greil, G., T. Geva, S. Maier, and A. Powell, *Effect of acquisition parameters on the accuracy of velocity encoded cine magnetic resonance imaging blood flow measurements.* Journal of Magnetic Resonance Imaging, 2002. 15(1): p. 47-54.

98. McKinnon, G., J. Debatin, D. Wetter, and G. von Schulthess, *Interleaved echo planar flow quantitation.* Magnetic Resonance in Medicine, 1994. 32(2): p. 263-267.

99. Debatin, J., D. Leung, S. Wildermuth, R. Botnar, J. Felblinger, and G. McKinnon, *Flow quantitation with echo-planar phase-contrast velocity*

mapping: in vitro and in vivo evaluation. Journal of Magnetic Resonance Imaging, 1995. 5(6): p. 656-662.

100. Mohiaddin, R., P. Gatehouse, and D. Firmin, *Exercise-related imaging changes in aortic flow measured with spiral echo-planar MR velocity mapping.* Journal of Magnetic Resonance Imaging, 1995. 5(2): p. 159-163.

101. Bock, M., S. Schoenberg, L. Schad, M. Knopp, M. Essig, and G. van Kaick, *Interleaved gradient-echo planar (IGEPI) and phase contrast CINE-PC flow measurements in the renal artery.* Journal of Magnetic Resonance Imaging, 1998. 8(4): p. 889-895.

102. Thomsen, C., M. Cortsen, L. Sondergaard, O. Henriksen, and S. F, *A segmented K-space velocity mapping protocol for quantification of renal artery blood flow during breath-holding.* Journal of Magnetic Resonance Imaging, 1995. 5(4): p. 393-401.

103. Chuang, M., M. Chen, V. Khasgiwala, M. McConnell, R. Edelman, and W. Manning, *Adaptive correction of imaging plane position in segmented k-space cine cardiac MRI.* Journal of Magnetic Resonance Imaging, 1997. 7(5): p. 811-814.

104. Davis, C., P. Liu, M. Hauser, S. Gohde, G. von Schulthess, and J. Debatin, *Coronary flow and coronary flow reserve measurements in humans with breath-held magnetic resonance phase contrast velocity mapping.* Magnetic Resonance in Medicine, 1997. 37(4): p. 537-544.

105. Laffon, E., R. Lecesne, V. de Ledinghen, N. Valli, P. Couzigou, F. Laurent, J. Drouillard, D. Ducassou, and L. Barat, *Segmented 5 versus nonsegmented flow quantitation: comparison of portal vein flow measurements.* Investigative Radiology, 1999. 34(3): p. 176-180.

106. Zhang, H., S. Halliburton, J. Moore, O. Simonetti, P. Schvartzman, R. White, and G. Chatzimavroudis, *Accurate quantification of steady and pulsatile flow with segmented k-space magnetic resonance velocimetry.* Experiments in Fluids, 2002. 33(1): p. 458-463.

107. Chatzimavroudis, G., H. Zhang, S. Halliburton, J. Moore, O. Simonetti, P. Schvartzman, A. Stillman, and R. White, *Clinical blood flow quantification with segmented k-space magnetic resonance phase velocity mapping.* Journal of Magnetic Resonance Imaging, 2003. 17(1): p. 65-71.

108. Frank, A., K. Selby, R. van Tyen, B. Nordell, and D. Saloner, *Cardiac-gated MR angiography of pulsatile flow: k-space strategies.* Journal of Magnetic Resonance Imaging, 1995. 5(3): p. 297-307.

109. Maier, S., M. Scheidegger, K. Liu, and P. Boesiger, *Accurate velocity mapping with FAcE.* Magnetic Resonance in Medicine, 1996. 14(2): p. 163-171.

110. Lewis, J., L. Kuo, J. Nelson, M. Limacher, and M. Quinones, *Pulsed Doppler echocardiographic determination of stroke volume and cardiac output: clinical*

validation of two new methods using the apical window. Circulation, 1984. 70(3): p. 425-431.

111. Skjaerpe, T., L. Hegrenaes, and L. Hatle, *Noninvasive estimation of valve area in patients with aortic stenosis by Doppler ultrasound and two-dimensional echocardiography.* Circulation, 1985. 72(4): p. 810-818.

112. Lanzer, P., C. Barta, E. Botvinick, H. Wiesendanger, G. Modin, and C. Higgins, *ECG-synchronized cardiac MR-imaging: method and evaluation.* Radiology, 1985. 155(3): p. 681-686.

113. Wendt, R., R. Rokey, G. Vick, and D. Johnston, *Electrocardiographic gating and monitoring in NMR imaging.* Magnetic Resonance Imaging, 1988. 6(1): p. 89-95.

114. Fischer, S., S. Wickline, R. Setser, M. Hofman, and C. Lorenz. *Vectorcardiographic investigation of the magnetohydrodynamic ECG artifact and aortic blood flow and large vessel geometry obtained by MRI*. in *Proceeding of the 6th Annual Meeting of International Society for Magnetic Resonance in Medicine*. 1998. Sydney, Australia.

115. Larson, A., R. White, G. Laub, E. McVeigh, D. Li, and O. Simonetti, *Self-gated cardiac cine MRI.* Magnetic Resonance in Medicine, 2004. 51(1): p. 93-102.

116. Runge, V., J. Clanton, C. Partain, and A.J. James, *Respiratory gating in magnetic resonance imaging at 0.5 Tesla.* Radiology, 1984. 151(2): p. 521-523.

117. Sakuma, H., N. Fujita, T. Foo, G. Caputo, S. Nelson, J. Hartiala, A. Shimakawa, and C. Higgins, *Evaluation of left ventricular volume and mass with breath-hold cine MR imaging.* Radiology, 1993. 188(2): p. 377-380.

118. Enzmann, D., M. Marks, and N. Pelc, *Comparison of cerebral artery blood flow measurements with triggered cine and non-triggered 2 D phase-contrast techniques.* Journal of Magnetic Resonance Imaging, 1993. 3: p. 705-712.

119. Papaharilaou, Y., D. Doorly, and S. Sherwin, *Assessing the accuracy of two-dimensional phase-contrast MRI measurements of complex unsteady flows.* Journal of Magnetic Resonance Imaging, 2001. 14: p. 714-723.

120. Arheden, H., M. Saeed, E. Törnqvist, G. Lund, M. Wendland, C. Higgins, and F. Ståhlberg, *Accuracy of segmented MR velocity mapping to measure small vessel pulsatile flow in a phantom simulating cardiac motion.* Journal of Magnetic Resonance Imaging, 2001. 13(5): p. 722-728.

121. Frayne, R. and B. Rutt, *Understanding acceleration-induced displacement artifacts in phase-contrast MR velocity measurements.* Journal of Magnetic Resonance Imaging, 1995. 5(2): p. 207-215.

122. Wolf, R.L., R.L. Ehman, S.J. Riederer, and P.J. Rossman, *Analysis of systematic and random error in MR volumetric flow measurements.* Magnetic Resonance in Medicine, 1993. 30(1): p. 82-91.

123. Hamilton, C., P. Moran, P. Santago, and S. Rajala, *Effects of intravoxel velocity distribution on the accuracy of the phase-mapping method in phase-contrast MR angiography.* Journal of Magnetic Resonance Imaging, 1994. 4(5): p. 752-755.

124. Oshinski, J.N., D.N. Ku, and R.I. Pettigrew, *Turbulent fluctuation velocity: the most significant determinant of signal loss in stenotic vessels.* Magnetic Resonance in Medicine, 1995. 33(2): p. 193-199.

125. Steinman, D., C. Ethier, and B. Rutt, *Combined analysis of spatial and velocity displacement artifacts in phase contrast measurements of complex flows.* Journal of Magnetic Resonance Imaging, 1997. 7(2): p. 339-346.

126. von Schulthess, G. and C. Higgins, *Blood flow imaging with MR: spin-phase phenomena.* Radiology, 1985. 157(3): p. 687-695.

127. Kouwenhoven, M., M. Hofman, and M. Sprenger, *Motion induced phase shifts in MR: acceleration effects in quantitative flow measurements--a reconsideration.* Magnetic Resonance in Medicine, 1995. 33(6): p. 766-777.

128. Frank, L., A. Crawley, and R. Buxton, *Elimination of oblique flow artifacts in magnetic resonance imaging.* Magnetic Resonance in Medicine, 1992. 25(2): p. 299-307.

129. Nishimura, D., J. Jackson, and J. Pauly, *On the nature and reduction of the displacement artifact in flow images.* Magnetic Resonance in Medicine, 1991. 22(2): p. 481-492.

130. Simonetti, O., R.I. Wendt, and J. Duerk, *Significance of the point of expansion in interpretation of gradient moments and motion sensitivity.* Journal of Magnetic Resonance Imaging, 1991. 1(5): p. 569-577.

131. Kilner, P., D. Firmin, R. Rees, J. Martinez, D. Pennell, R. Mohiaddin, S. Underwood, and D. Longmore, *Valve and great vessel stenosis: assessment with MR jet velocity mapping.* Radiology, 1991. 178(1): p. 229-235.

132. Ståhlberg, F., C. Thomsen, L. Søndergaard, and O. Henriksen, *Pulse sequence design for MR velocity mapping of complex flow: notes on the necessity of low echo times.* Magnetic Resonance in Medicine, 1994. 12(8): p. 1255-1262.

133. Conturo, T. and G. Smith, *Signal-to-noise in phase angle reconstruction: dynamic range extension using phase reference offsets.* Magnetic Resonance in Medicine, 1990. 15(3): p. 420-437.

134. Polzin, J., F. Korosec, K. Wedding, T. Grist, R. Frayne, D. Peters, and C. Mistretta, *Effects of through-plane myocardial motion of phase-difference and complex-difference measurements of absolute coronary artery flow.* Journal of Magnetic Resonance Imaging, 1996. 6(1): p. 113-123.

135. Buonocore, M. and H. Bogren, *Factors influencing the accuracy and precision of velocity-encoded phase imaging.* Magnetic Resonance in Medicine, 1992. 26(1): p. 141-154.

136. Andersen, A. and J. Kirsch, *Analysis of noise in phase contrast MR imaging.* Medical Physics, 1996. 23(6): p. 857-868.

137. Hofman, M., A. van Rossum, M. Sprenger, and N. Westerhof, *Assessment of flow in the right human coronary artery by magnetic resonance phase contrast velocity measurement: effects of cardiac and respiratory motion.* Magnetic Resonance in Medicine, 1996. 35(4): p. 521-531.

138. Hofman, M., S. Wickline, and C. Lorenz, *Quantification of in-plane motion of the coronary arteries during the cardiac cycle: implications for acquisition window duration for MR flow quantification.* Journal of Magnetic Resonance Imaging, 1998. 8(3): p. 568-576.

139. Tang, C., D. Blatter, and D. Parker, *Accuracy of phase-contrast flow measurements in the presence of partial-volume effects.* Journal of Magnetic Resonance Imaging, 1993. 3(2): p. 377-385.

140. Tang, C., D. Blatter, and D. Parker, *Correction of partial-volume effects in phase-contrast flow measurements.* Journal of Magnetic Resonance Imaging, 1995. 5(2): p. 175-180.

141. d'Othee, B., G. Rachmuth, J. Munasinghe, and E. Lang, *The effect of hyperoxygenation on T1 relaxation time in vitro. Academic Radiology*, 2003. 10(8): p. 854-860.

142. Cloutier, G., L. Allard, Z. Guo, and L.-G. Durand, *The effect of averaging cardiac Doppler spectrograms on the reduction of their amplitude variability.* Medical And Biological Engineering And Computing, 1992. 30(2): p. 177-186.

143. Kessler, W., W. Moshage, A. Galland, D. Zink, S. Achenbach, W. Nitz, G. Laub, and K. Bachmann, *Assessment of coronary blood flow in humans using phase difference MR imaging. Comparison with intracoronary Doppler flow measurement.* International Journal of Cardiac Imaging, 1998. 14(3): p. 179-186.

144. Grist, T., J. Polzin, J. Bianco, T. Foo, M. Bernstein, and C. Mistretta, *Measurement of coronary blood flow and flow reserve using magnetic resonance imaging.* Cardiology, 1997. 88(1): p. 80-89.

145. Sakuma, H., L. Blake, T. Amidon, M. O'Sullivan, D. Szolar, A. Furber, M. Bernstein, T. Foo, and C. Higgins, *Coronary flow reserve: noninvasive measurement in humans with breath-hold velocity-encoded cine MR-imaging.* Radiology, 1996. 198(3): p. 745-750.

146. Hangiandreou, N., P. Rossman, and S. Riederer, *Analysis of MR phase-contrast measurements of pulsatile velocity waveforms.* Journal of Magnetic Resonance Imaging, 1993. 3(2): p. 387-394.

147. Li, H., G. Clarke, M. NessAiver, H. Liu, and R. Peshock, *Magnetic resonance imaging k-space segmentation using phase-encoding groups: The accuracy of quantitative measurements of pulsatile flow.* Medical Physics, 1995. 22(4): p. 391-399.

148. Kupari, M., P. Hekali, P. Keto, V.-P. Poutanen, L. Porkka, H. Turto, M. Nieminen, L. Toivonen, T. Ikonen, M. Ventilä, and L. Heikkilä, *Assessment of aortic valve area in aortic stenosis by magnetic resonance imaging.* The American Journal of Cardiology, 1992. 70(9): p. 952-955.

149. Kupari, M., P. Hekali, P. Keto, V.-P. Poutanen, M.J. Tikkanen, and C.-G. Standertskjöld-Nordenstam, *Relation of aortic stiffness to factors modifying the risk of atherosclerosis in healthy people.* Arteriosclerosis and Thrombosis, 1994. 14(3): p. 386-394.

150. Foo, T., M. Bernstein, A. Aisen, R. Hernandez, B. Collick, and T. Bernstein, *Improved ejection fraction and flow velocity estimates with use of view sharing and uniform repetition time excitation with fast cardiac techniques.* Radiology, 1995. 195(2): p. 471-478.

151. Moon, J., C. Lorenz, J. Frances, G. Smith, and D. Pennell, *Breath-hold FLASH and FISP cardiovascular imaging: Left ventricular volume differences and reproducibility.* Radiology, 2002. 223: p. 789-797.

152. Burkart, D., J. Felmlee, C. Johnson, R. Wolf, A. Weaver, and R. Ehman, *Cine phase-contrast MR flow measurements: improved precision using an automated method of vessel detection.* Journal of Computer Assisted Tomography, 1994. 18(3): p. 469-475.

153. Yang, G., P. Burger, P. Killner, S. Karwatowski, and D. Firmin, *Dynamic range extension of cine velocity measurements using motion-registered spatiotemporal phase unwrapping.* Journal of Magnetic Resonance Imaging, 1996. 6(3): p. 495-502.

154. Xiang, Q., *Temporal phase unwrapping for CINE velocity mapping.* Journal of Magnetic Resonance Imaging, 1995. 5(5): p. 529-534.

155. Markl, M. and J. Hennig, *Phase contrast MRI with improved temporal resolution by view sharing: k-space related velocity mapping properties.* Magnetic Resonance Imaging, 2001. 19(5): p. 669-676.

156. Sodickson, D. and W. Manning, *Simultaneous acquisition of spatial harmonics (SMASH): fast imaging with radiogfrequence coil arrays.* Magnetic Resonance in Medicine, 1997. 38(4): p. 591-603.

157. Pruessmann, K., M. Weiger, M. Scheidegger, and P. Boesinger, *SENSE: sensitivity encoding for fast MRI.* Magnetic Resonance in Medicine, 1999. 42(5): p. 952-962.

158. Thunberg, P., M. Karlsson, and L. Wigström, *Accuracy and reproducibility in phase contrast imaging using SENSE.* Magnetic Resonance in Medicine, 2003. 50(5): p. 1061-1068.

159. Alley, M., Y. Amano, R. Shifrin, N. Pelc, and R. Herfkens. *3D cine cardiac ventriculography with an Iron Oxide blood pool agent*. in *Proceeding of the 6th Annual Meeting of International Society for Magnetic Resonance in Medicine*. 1998. Sydney, Australia.

160. Francis, J., J. Moon, and G. Smith. *The benefit of TrueFISP versus FLASH imaging in patients with poor left ventricular function.* in *Fourth Annual Meeting of the Society for Cardiovascular Magnetic Resonance*. 2001.

161. Merrifield, R., J. Keegan, D. Firmin, and G. Yang. *Dual RF flip angle TrueFISP cardiovascular MRI*. in *Proceeding of the 9th Annual Meeting of International Society for Magnetic Resonance in Medicine*. 2001. Glasgow, Scotland.

162. Alley, M., S. Nabel, Y. Amano, D. Paik, R. Shifrin, A. Shimakawa, N. Pelc, and R. Herfkens, *Fast 3D cardiac cine MR imaging.* Journal of Magnetic Resonance Imaging, 1999. 9(5): p. 751-755.

163. Scheffler, K. *3D cardiac cine imaging in a single breath-hold using elliptically reordered 3D trueFISP*. in *Proceedings of the 9th Annual Meeting of ISMRM*. 2001. Glasgow, Scotland.

164. Jung, B., J. Hennig, and K. Scheffler, *Single-breathhold 3D-trueFISP cine cardiac imaging.* Magnetic Resonance in Medicine, 2002. 48(5): p. 921-925.

165. Hinton, D., L. Wald, J. Pitts, and F. Schmitt, *Comparison of cardiac MRI on 1.5 T and 3.0 Tesla clinical whole body systems.* Investigive Radiology, 2003. 38(7): p. 436-442.